Study on Polyphenylene Ionomer Membranes

A Doctoral Thesis

Presented to Energy Materials Science

Integrated Graduated School of

Medicine, Engineering and Agricultural Science

University of Yamanashi

March 2021

Keisuke Shiino

Contents

Chapter 1 General Introduction

1.1 Environmental problems

Since the industrial revolution, we have obtained comfortable life. Science and technology has been drastically improved accompanying with increasing energy consumption, mostly from fossil fuels. Even in the 21st century, we rely heavily on fossil fuels as primary energy resources, however, Japan is an island country geometrically separated from other countries via seas and has insufficient mining resources such as petroleum oil or coal. We have imported plenty of such resources from overseas, and the self-sufficiency rate of primary energy is less than 10%, the second lowest among the developed countries in 2017 [(1)]. Especially, we have imported petroleum oil mostly from middle-east, thus, it has been difficult to be suppled at a stable price because of influence of international affairs [(2)]. Moreover, fossil fuels emit harmful gases such as CO_2, NO_x or SO_x at conventional power plants or internal combustion vehicles, which have caused global warming or environmental pollution. At the same time, depletion of fossil fuels is another crucial issue of humankind. To address these problems, power generation by nuclear power plant has increased, however, the catastrophe caused by the accident of Fukushima nuclear power plant due to Great East Japan Earthquake has made it difficult for Japan to accept the nuclear power plants. In 2017, Japan exhausted greenhouse gas more than 1.5 billion tons in total, the fifth largest in the world, and we have set the goal after Paris agreement to reduce greenhouse gas emissions by 26% (2030) and by 80 % (2050) from the level in 2013 [(3)].

Japanese government has formulated ”3E+S” to achieve Energy security, Economic efficiency and Environment simultaneously based on Safety. For this purpose, clean

power generator with renewable energy such as solar or wind power has become more and more important. Furthermore, spreading the renewable energy would stimulate the market of electricity bidirectionally (buying and selling). However, the electricity made out of such renewable energy has two major issues. Firstly, large renewable energy power plants need large area with some specific geographical requirements, thus they usually are located far from large energy consumption area. For transporting the electricity to a distant place, the electricity is lost as vibration or heat due to the resistance at the substation and electrical wire (i.e., transmission loss). Secondly, the stability is always a problem because the solar or wind power plant depends on the natural environments such as the sunshine duration or wind speed. The stable power supply solely from renewable energy is generally difficult.

1.2 Hydrogen

Hydrogen can be produced by various methods such as water electrolysis or steam reforming. Currently, hydrogen is mostly produced by reformation of the city gas or liquefied petroleum gas. In addition, plenty of hydrogen is produced as a by-product during the steel manufacture. In the future, hydrogen should be produced by water electrolysis using excessive electricity at renewable energy power plants (e.g., at solar power plants during the day time). By transporting the hydrogen to consumption area and storing until night time when the solar power cannot work and electricity demand is increased, high energy utilization efficiency can be accomplished. This is similar situation found in other renewable energy such as wind, water or geothermal power. Hydrogen can generate electricity via fuel cells with less amount of harmful gases than those of conventional thermal power plants. This cycle, hydrogen production, transportation,

storage and utilization is called “Hydrogen Society”. In order to achieve the hydrogen society in the future, it is important to improve the performance of the fuel cells as key devices [4].

1.3 Polyphenylene

Polyphenylenes are one of the simplest polymers. Generally, polyphenylenes consist of phenylene rings in the main chains, and may contain side chains (alkyl, phenyl groups etc). Due to the π-conjugated characteristics, polyphenylenes have been used in applications such as organic electronic devices, sensors, fluorescent tags, etc [5, 6].

Polyphenylenes have relatively long history. In the 1960s, unsubstituted poly(*p*-phenylene)s were synthesized from benzene using aluminum(III) chloride as a Lewis acid catalyst and copper(II) chloride as an oxidant[7, 8], known as Scholl reaction. To obtain more structurally defined polyphenylenes, some emerging aryl-aryl coupling reactions, such as Ullmann [9, 10], Kumada [11, 12], Yamamoto [13, 14], Negishi [15, 17], Stille [18, 19] and Suzuki [20, 22] methods, have been applied (Scheme 1-1) [23]. Polyphenylenes can also be synthesized without metal catalyst. For example, Diels−Alder cycloaddition reaction of an ethynyl-substituted aryl compound with a cyclopentadienone via a 4 + 2 mechanism provides polyphenylenes (Scheme 1-2) [24-26].

Recently, polyphenylenes functionalized with sulfonic acid groups have attracted significant interests as proton exchange membranes (PEMs) because of its excellent thermal and chemical stabilities. Sulfonated polyphenylenes have high potentials as alternative membranes to state-of-the-art perfluorinated ionomer membranes in PEMFCs.

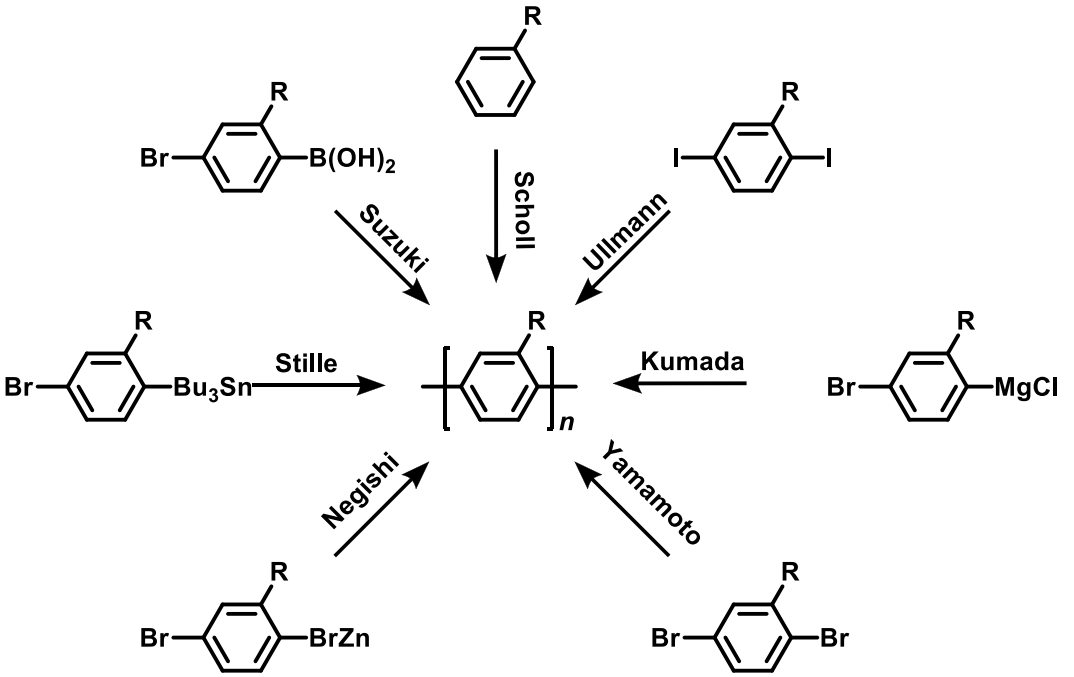

Scheme 1-1 Synthesis of polyphenylenes via transition metal cross-coupling reactions.

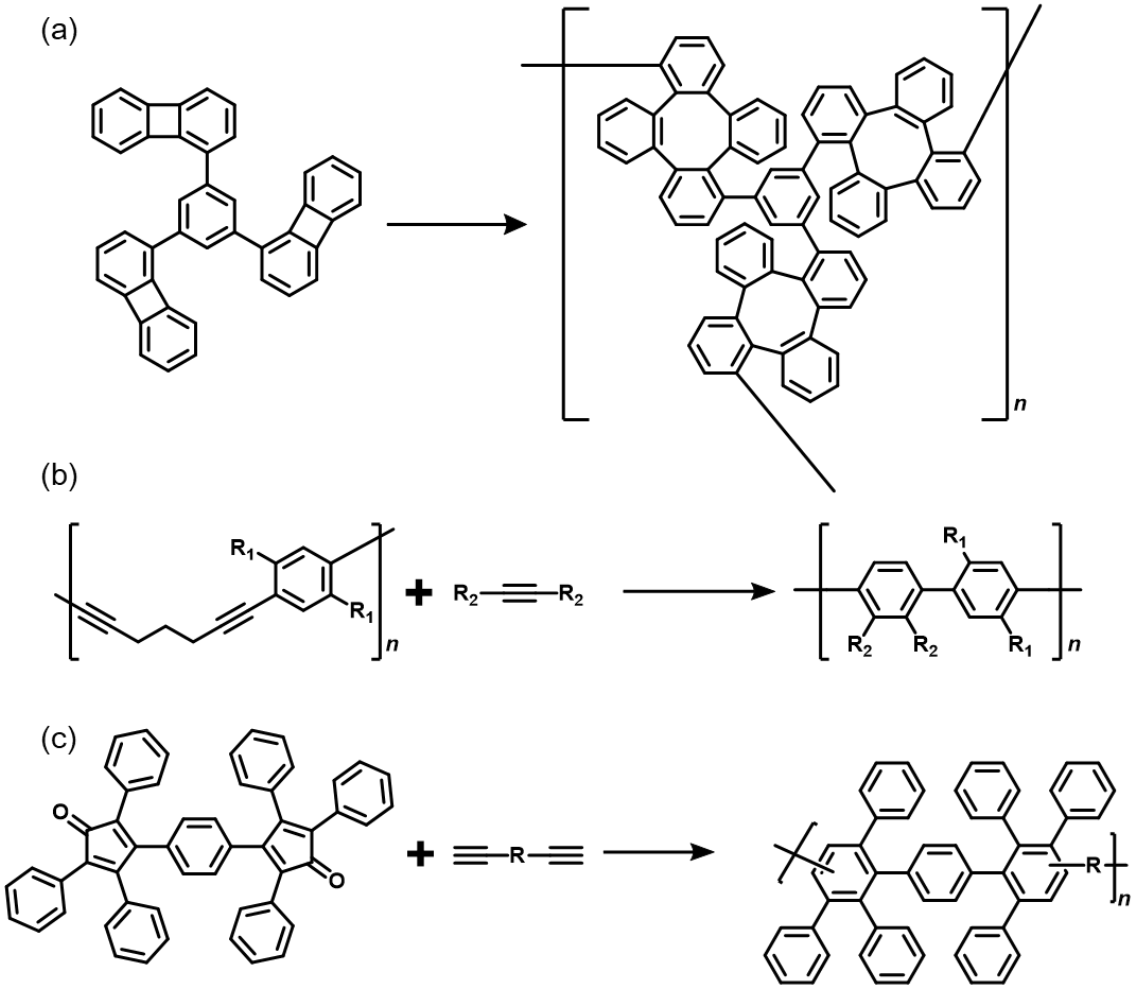

Scheme 1-2 Synthesis of polyphenylenes without metal catalyst.

1.4 Sulfonated polyphenylene ionomer

There have been several papers claiming that polyphenylene functionalized by sulfonic acid group can be used as PEMs in polymer electrolyte membrane fuel cells (PEMFCs) because they potentially have 1) high proton conductivity 2) low gas permeability coefficient 3) low environmental load 4) low production cost compared with the conventional perfluorinated PEMs, 5) good oxidative stability and 6) outstanding thermal tolerance. To be more specific, regarding 1), polyphenylene-based PEMs can have high sulfonic acid group density (or high ion exchange capacity (IEC)), leading to high proton conductivity comparable to or much higher than that of the conventional perfluorinated PEMs. This facilitates efficient proton conduction during fuel cell power generation. Regarding 2), fuel (i.e., hydrogen) and oxidant (i.e., oxygen) are supplied to anode and cathode, and they must be separated by the electrolyte. Most aromatic polymers are known to have low gas permeability coefficient. Regarding 3) and 4), for wide spread dissemination of fuel cells, it is necessary to reduce the environmental impact and production cost. The use of fluorine-free PEMs may lead to HF-emission-free when discarding PEMFCs [(27)]. In addition, aromatic PEMs can be produced from low-cost petrochemicals more easily than the perfluorinated PEMs. Regarding 5) it is widely accepted that chemical degradation of the conventional sulfonated aromatic hydrocarbon ionomer membranes takes place on heteroatom linkages by the attack of hydroxyl ($HO^{\bullet}$) and hydroperoxyl ($HOO^{\bullet}$) radicals as by-product of ORR [(28)]. Since polyphenylenes do not carry chemically vulnerable part in the backbone, chemical degradation is unlikely to occur. Regarding 6) the energy conversion efficiency of PEMFCs is improved with increasing temperature. In low temperature PEMFCs (ca. 80 ^{o}C), large amount of heat is produced during operation and must be removed to maintain the operating temperature

by cooling systems. In contrast, high temperature operation (120-160 ^{o}C) allows easy heat management due to the greater temperature difference between the operating temperature and the ambient environment. Consequently, cooling system is simplified, power density is improved, and overall system efficiency is increased [29, 30]. Higher thermal tolerance properties of sulfonated polyphenylene ionomer membrane compared to that of conventional PEMs allows to increase the operation temperature, resulting in improving energy conversion efficiency [31].

Rikukawa *et al.* claimed that they successfully synthesized poly(*p*-phenylene) having pendant sulfonic benzene diblock copolymer and narrow polydispersity index via Kumada coupling reaction using Ni catalyst [32]. The high molecular weight was achieved with hydrophobic monomer protected by a neopentyl group. The proton conductivity of their polyphenylene ionomer membrane (IEC = 2.16 mequiv. g^{-1}) was comparable (ca. over than 0.1 mS cm^{-1} at 80 ^{o}C and 90% RH) to NRE 112 despite the IEC lower than the conventional aromatic PEMs due to well-developed phase-separated morphology (Scheme 1-3).

Highly phenylated arylene-based sulfonated ionomer synthesized via Diels-Alder polymerization was also investigated by Douglas *et al* [33]. Post-sulfonation reaction successfully controlled the IEC, and resulting polymer provided homogeneous sulfonated membrane (Scheme 1-4). The membrane showed excellent chemical and thermal stability. The thermal decomposition of the sulfonic acid groups occurred below the glass transitional temperature (T_g), while the T_g of the unsulfonated polymer membrane was much higher (388 ^{o}C) than that of the perfluorinated ionomer PEMs.

However, the mechanical strength of these membranes were significantly low and insufficient (the elongations at break were 1.2% at 25 ^{o}C and 50% RH for the former, and

12% under dry condition for the latter, respectively) for application to PEMFCs.

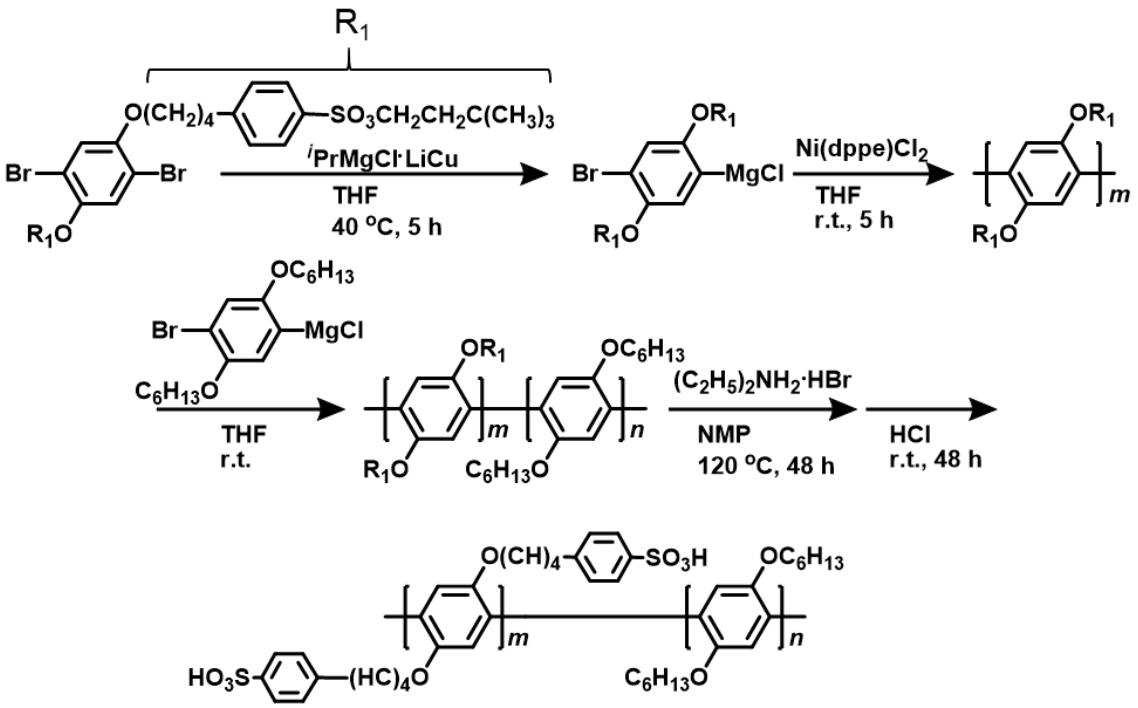

Scheme 1-3 Synthesis of poly(*p*-phenylene) membrane with pendant sulfonic benzene diblock copolymer.

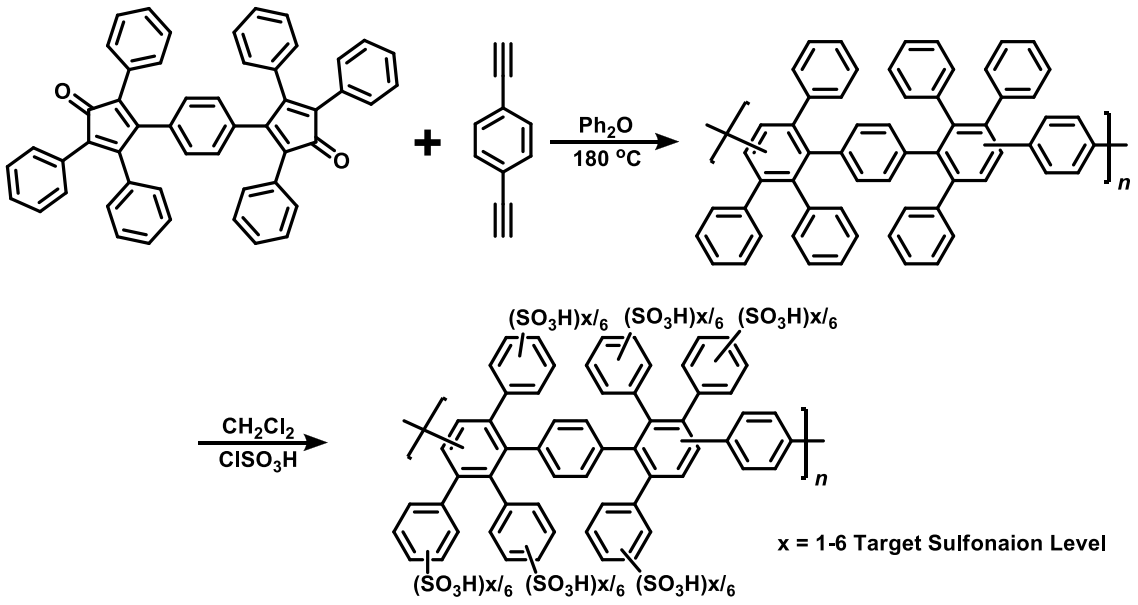

Scheme 1-4 Synthesis of highly phenylated polyphenylene membrane with pendant sulfonic benzene diblock copolymer.

1.5 Mechanical strength for PEMs

Mechanical strength and flexibility is another important properties for lifetime of PEMFCs. Aromatic PEMs generally exhibit high strength, but insufficient flexibility due to its rigid molecular structure. They tend to absorb large amount of water at high humidity, which results in low dimensional stability. In PEMFCs operation, PEM is frequently exposed to dry and wet conditions mostly depending on the operating current density because fuel cell reaction of oxygen and hydrogen produces water. Thus, PEMs should have high mechanical strength to withstand the dry-wet cycles [34].

To achieve sufficiently high mechanical properties, chemical stability, and proton conductivity simultaneously, our laboratory developed the simple polyphenylene ionomer, SPP-QP, consisted of quinque-phenylene (five consecutive phenylene) groups as hydrophobic component and sulfonated phenylene as hydrophilic component without any side-chains and other substituents (Figure 1-1. This polyphenylene ionomer membrane showed high proton conductivity comparable to Nafion, high chemical stability and reasonable mechanical properties, in particular elongation at break (68%) by the novel polymer design principle based on the persistence length (l_p), which is the characteristic length scale for the exponential decay of the correlation of main-chain tangent [35]. In other word, l_p describes the length for backbone to bend by 90 ^{o} on average. Although SPP-QP showed excellent properties among the polyphenylene ionomer PEMs, there still remains questions such as whether the quinque-phenylene is the optimal hydrophobic structure for PEMs to be applied for PEMFCs.

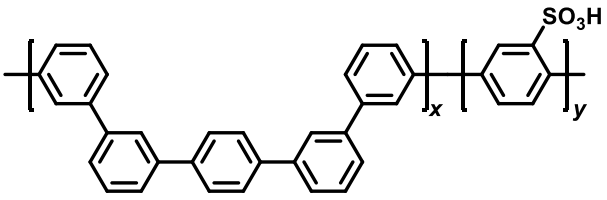

Figure 1-1 Chemical structure of sulfonated polyphenylene-quinquephenylene.

1.6 Objective of this research

Many efforts have been devoted to apply the sulfonated polyphenylene ionomer membrane to PEMFCs, however, no membranes have satisfied the all required properties. Our SPP-QP membranes seems the closest to the target goal, several issues still remain. The purpose of this PhD study is to reveal the structure/properties relationship in the polyphenylene ionomers for improving further proton conductivity, mechanical strength, especially elongation at break, for practical fuel cell operation. In this research, two factors are focused, the composition and sequence length of hydrophobic component (unsubstituted phenylene groups).

In chapter 2, the polyphenylene ionomer with different composition of biphenylene groups was synthesized, and its membrane forming capability was investigated. Based on the results, polyphenylene ionomer was synthesized from dichlorobenzene with the optimum composition for hydrophobic monomer, and its polymer properties such as molecular weight and randomness of the hydrophilic unit are discussed.

In chapter 3, the impact of the difference mentioned in chapter 2 on the membrane morphology was investigated using TEM observation, small angle X-lay scattering and small angle neutron scattering measurements. Structural models have been devised based on those analytical data. The relationship of morphology/properties such as proton conductivity and mechanical strength are discussed in details.

In chapter 4, to achieve better membrane properties, a process for synthesizing a polyphenylene ionomer with large sequence length of the hydrophilic unit was investigated. Specifically, the order of addition of hydrophobic monomer was changed. Lastly, new sequenced hydrophilic monomer was designed and applied for the copolymerization with the hydrophobic monomer.

1.7 References

(1) JAPAN'S ENERGY. 2019 published by “Ministry of Economy, Trade and Industry Agency for Natural Resources and Energy”

(2) Nuclear power pamphlet published by “Japan Atomic Energy Relations Organization”

(3) the Energy Data and Modelling Center, the Institute of Energy Economics, Japan, Energy Conservation Center EDMC handbook of Japan's & world energy & economic statistics. (2020)

(4)Hydrogen energy white paper published by New Energy and Industrial Technology Development Organization (NEDO)

(5) Hammer, B. A. G.; Müllen, K. *Chem. Rev.* **2016**, *116*, 2103-2140.

(6) Liu, D.; Feyter, S. D.; Cotlet, M.; Stefan, A.; Wiesler, U.-M.; Herrmann, A.; Koehler, D. G.; Qu, J.; Mü1llen, K.; Schryver, F. C. D. *Macromolecules* **2003**, *36*, 5918-5925.

(7) Kovacic, P.; Kyriakis, A. *Tetrahedron Lett.* 1962, *3*, 467-769.

(8) Zhai, L.; Shukla, R.; Wadumethrige, S. H; Rathore, R. *J. Org. Chem.* **2010**, *75*, 4748-4760.

(9) Claesson, V. S.; Gehm, R.; Kern, W. *Makromol. Chem.* **1951**, *7*, 46−61.

(10) Giri, R.; Brusoe, A.; Troshin, K.; Wang, J. Y.; Font, M.; Hartwig, J. F. *J. Am. Chem. Soc.* **2018**, *140*, 793-806.

(11) Tamao, K.; Sumitani, K.; Kumada, M. *J. Am. Chem. Soc.* **1972**, *94*, 4374 -4376.

(12) Dawson, D. D.; Oswald, V. F.; Borovik, A. S.; Jarvo, E. R. *Chem. Eur. J.* **2020**, *26*, 3044-3048.

(13) Yamamoto, T.; Wakabayashi, S.; Osakada, K. *J. Organomet. Chem.* **1992**, *428*, 223−237.

(14) Asakura, H.; Shishido, T.; Tanaka, T. *J. Phys. Chem. A* **2012**, *116*, 4029-4034.

(15) King, A. O.; Okukado, N.; Negishi, E.-i. *J. Chem. Soc., Chem. Commun.* **1977**, *19*, 683−684.

(16) Phapalea, V. B.; Cárdenas, D. *J. Chem. Soc. Rev.* **2009**, *38*, 1598-1607.

(17) Gioria, E.; Martínez-Ilarduya, J.; Espinet, P. *Organometallics* **2014**, *33*, 4394-4400.

(18) Milstein, D.; Stille, J. K. *J. Am. Chem. Soc.* **1978**, *100*, 3636-3638.

(19) Russell, J. E. A.; Entz, E. D.; Joyce, I. M.; Neufeldt, S. R. *ACS Catal.* **2019**, *9*, 3304-3310.

(20) Miyaura, N.; Yamada, K.; Suzuki, A. *Tetrahedron Lett.* **1979**, *20*, 3437-3440.

(21) Schluter, A. D. *J. Polym. Sci., Part A: Polym. Chem.* **2001**, *39*, 1533-1556.

(22) Yokozawa, T.; Kohno, H.; Ohta, Y.; Yokoyama, A. *Macromolecules* **2010**, *43*, 7095-7100.

(23) Sherwood, J.; Clark, J. H.; Fairlamb, I. J. S.; Slattery, J. M. *Green Chem.* **2019**, *21*, 2164-2213.

(24) Mindach, L.; Müllen, K. *Adv. Mater.* **1996**, *8*, 504−507.

(25) Batson, J. M.; Swager, T. M. *ACS Macro Lett.* **2012**, *1*, 1121–1123.

(26) Budy, S. M.; Khan, M.; Chang, X.; Iacono, S. T.; Son, D. Y. *J. Polym. Sci.* **2020**, *58*, 2774-2783.

(27) Peighambardoust, S. J.; Rowshanzamir, S.; Amjadi, M. *Int. J. Hydrogen Energy* **2010**, *35*, 9349-9384.

(28) Zhang, L.; Mukerjee, S. *J. Electrochem. Soc.* **2006**, *153*, A1062-A1072.

(29) Zhang, J.; Xie, Z.; Zhang, J.; Tang, Y.; Song, C.; Navessin, T.; Shi, Z.; Song, D.; Wang, H.; Wilkinson, D. P.; Liu, Z.-S.; Holdcroft, S. *J. Power Sources* **2006**, *160*, 872-891.

(30) Escorihuela, J.; Olvera-Mancilla, J.; Alexandrova, L.; Castillo, L. F. d.; Compañ, V.

Polymers **2020**, *12*, 1861-1901.

(31) Lee, H.-F.; Huang, Y.-C.; Wang, P.-H.; Lee, C. C.; Hung, Y.-S.; Gopal, R.; Holdcroft, S.; Huang, W.-Y. *Mater. Today Commun.* **2015**, *3*, 114-121.

(32) Takeoka, Y.; Umezawa, K.; Oshima, T.; Yoshida, M.; Yoshizawa-Fujita, M.; Rikukawa, M. *Polym. Chem.* **2014**, *5*, 4132-4140.

(33) Fujimoto, C. H.; Hickner, M. A.; Cornelius, C. J.; Loy, D. A. *Macromolecules* **2005**, *38*, 5010-5016.

(34) Yoo, J.; Jang, H.; Sutradhar, S. C.; Ha, J.; Choi, K.; Ryu, T.; Yang, H.; Yoon, S.; Kim, W. *Int. J. Hydrogen Energy* **2017**, *42*, 1766-1775.

(35) Miyake, J.; Taki, R.; Mochizuki, T.; Shimizu, R.; Akiyama, R.; Uchida, M.; Miyatake, K. *Sci. Adv.* **2017**, *3*, eaao0476.

Chapter 2 Sulfonated Polyphenylenes: Novel Synthetic Methods

2.1 Introduction

Ion conductive polymers have been extensively investigated for applications such as sensors, actuators, and batteries [1–3]. Among them, fuel cells using proton conductive polymer membranes have been recognized as alternative energy–converting devices due to the high efficiency and low environmental pollution. For fuel cell membranes, high proton conductivity, water transport capability, stability (e.g., thermal, mechanical, chemical), gas impermeability, and compatibility with catalyst layers are required. Perfluorosulfonic acid (PFSA) ionomers, such as Nafion, have been most used as fuel cell membranes due to the balanced properties in terms of proton conductivity, and mechanical and chemical stability [4]. However, there still remain issues for PFSA membranes to be addressed, such as high gas permeability, low thermal stability (i.e., low glass-transition temperature), low environmental compatibility, and high production cost. Since most of them are intrinsic issues for perfluorinated polymeric materials, non-fluorinated ionomers with wide varieties of molecular structures have been extensively investigated in the last two decades [5-9]. Among the alternative membranes, sulfonated polyphenylenes, or polyphenylene ionomers, have been regarded as one of the most attractive and promising candidates due to the high chemical stability of the polymer backbones. For example, Holdcroft *et al.* reported that sulfophenylated polyphenylene membranes possessed high oxidative stability with no remarkable degradation after the accelerated stress testing (e.g., Fenton's test at 80 °C for 1 h) [10, 11]. More recently, we

reported that a new and simpler version of sulfonated polyphenylene (SPP-QP, Figure 1-1) with no extra substituents provided thin membranes with bendability, high proton conductivity, high gas barrier property, and excellent chemical stability [(12)]. The SPP-QP membrane functioned well in an operating fuel cell with high performance and durability. SPP-QP used quinquephenylene (five consecutive phenylene) monomer as a hydrophobic component, which required two-step Suzuki-Miyaura coupling reaction for the synthesis. Herein, I propose a simpler, but practically cost-effective synthetic approach for polyphenylene ionomers. The novel polyphenylene ionomer, SPP-BP or SPP-MP, consists of sulfonated *p*-phenylene and unsubstituted *m*- and *p*-biphenylene groups or *m*- and *p*-monophenylene in the main chain, respectively. SPP-BP can be easily synthesized from readily available reagents, such as 3,3'-dichlorobiphenyl (BP_{mm}), 4,4'-dichlorobiphenyl (BP_{pp}) and 2,5-dichlorobenzenesulfonic acid (SP) monomers. SPP-MP can be also synthesized from commercialized 1,3-dichlorobenzene (MP_m), 1,4-dichlorobenzene (MP_p) and SP monomer. For the monomer synthesis, it is noteworthy that ca. 70% for BP and 98% for MP monomer of the raw materials cost can be reduced, compared with that of SPP-QP, although, the amount of $Ni(cod)_2$ is increased with introducing simple monomer. The synthetic process for the BP monomers (i.e., two parallel steps) and MP monomer (i.e., commercial usage) may further reduce the cost, compared with that for the QP monomer (i.e., two consecutive steps).

2.2 Experimental

2.2.1 Chemicals

m-Dichlorobenzene, *p*-dichlorobenzene, 1-chloro-3-iodobenzene, and 1-chloro-4-iodobenzene were purchased from TCI, Inc. and used as received. Tetrakis(triphenylphosphine)palladium(0) [$Pd(PPh_3)_4$], 2,5-dichlorobenzenesulfonic acid dihydrate [SP monomer], 3-chlorophenylboronic acid, 4-chlorophenylboronic acid, bis(1,5-cyclooctadiene)nickel(0) [$Ni(cod)_2$], 2,2'-bipyridine, potassium carbonate [K_2CO_3], sodium carbonate [Na_2CO_3], magnesium sulfate [$MgSO_4$], dimethyl sulfoxide [DMSO], toluene, toluene dehydrate, methanol, 2-propanol, 0.01 M sodium hydroxide aqueous solution, hydrochloric acid, sulfuric acid, sodium chloride, hexane, chloroform-d_1 [$CDCl_3$], and deuterated dimethyl sulfoxide [DMSO-d_6] were purchased from Kanto Chemical Co. and used as received.

2.2.2 Measurements

^1H (500 MHz) and ^{13}C (125 MHz) NMR spectra were recorded on a JEOL JNM-ECA 500 spectrometer with $CDCl_3$ or DMSO-d_6 as a solvent and tetramethylsilane as an internal reference. Molecular weights of polymers were estimated from GPC equipped with a Jasco MD-4017 UV detector and a Shodex K-805L column at 50 ºC. DMF containing 0.01 M LiBr was used as an eluent. Molecular weight was calibrated with standard polystyrene samples. IEC of the membranes was calculated from acid base titration. A piece of membrane (ca. 20 mg) was immersed in 2 M NaCl aqueous solution for 12 h at room temperature. HCl released by the ion exchange reaction was titrated with a standard 0.01 M NaOH aqueous solution using automatic potentiometric titrator (AT-510, Kyoto electronics manufacturing Co., Ltd.) at room temperature.

2.2.3 Ion exchange of sodium 2,5-dichlorobenzenesulfonate (SP-Na^+ monomer)

A 100 mL three-neck flask was charged with SP-H^+ monomer (19.0 mmol, 5.00 g) and pure water (20 mL). To the solution, 5 M NaOH aqueous solution (5 mL) was added at room temperature. Then, the mixture was cooled in an ice bath to precipitate out SP-Na^+ monomer as a white solid. The SP-Na^+ monomer was collected by filtration and dried at 60 ºC in vacuum to obtain SP-Na^+ monomer (12.6 mmol, 3.14 g, 66.6% yield).

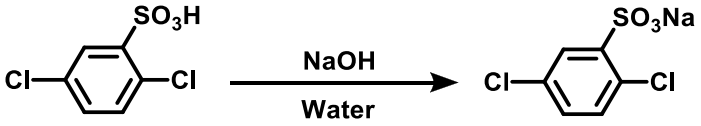

Scheme 2-1 Synthesis of SP-Na^+ monomer.

Synthesis of BP_{pp} monomer.

The BP_{pp} monomer was synthesized by Suzuki-Miyaura cross coupling reaction. A 300-mL three-neck round-bottomed flask equipped with a condenser, nitrogen inlet/outlet and magnetic stirring bar was charged with 4-chlorophenylboronic acid (7.82 g, 0.05 mol), 1-chloro-4-iodobenzene (11.9 g, 0.05 mol), 2 M aqueous Na_2CO_3 (75 mL), toluene (150 mL), and $Pd(PPh_3)_4$ (1.16 g, 0.001 mol). The mixture was stirred at 130 ºC for 21 h, cooled to room temperature, and then solution was recovered by filtration. After separation of two layers, the aqueous layer was extracted with toluene, and the combined organic layers were dehydrated using $MgSO_4$ and concentrated in vacuo. The crude product was purified by filtration with silica gel and recrystallization from 2-propanol. Pure BP_{pp} monomer was obtained as a white solid (9.79 g, 89.2%).

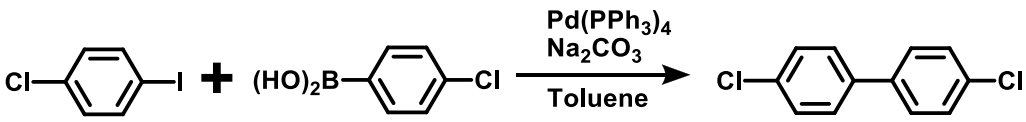

Scheme 2-2 Synthesis of BP_{pp} monomer.

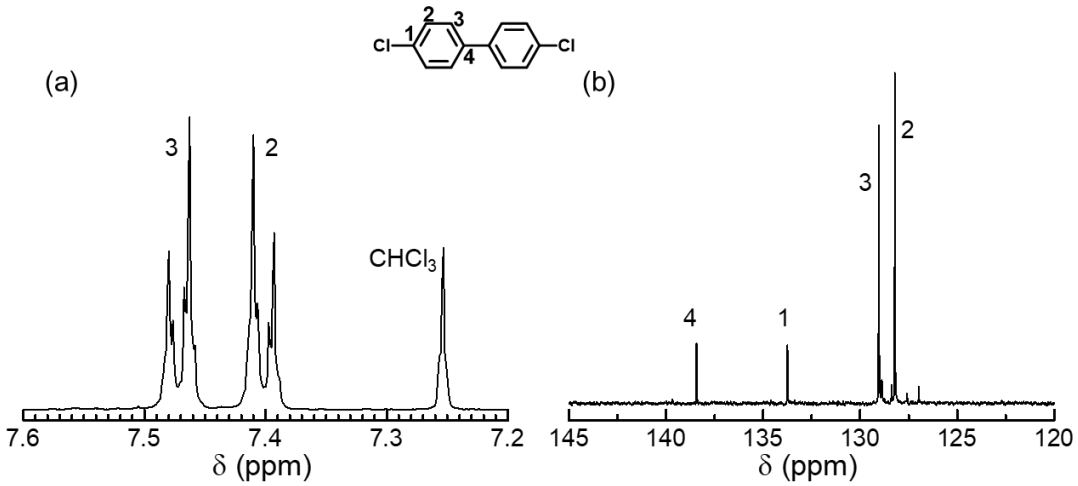

Figure 2-1 (a) ^{1}H and (b) ^{13}C NMR spectra of BP_{pp} monomer in $CDCl_3$ at r.t.

2.2.4 Synthesis of BP_{mm} monomer

The BP_{mm} monomer was synthesized under the similar reaction conditions with BP_{pp}. The BP_{mm} monomer was obtained as a transparent and colorless liquid (6.08 g, 69.1%).

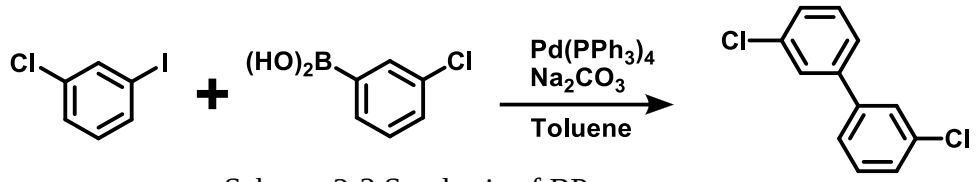

Scheme 2-3 Synthesis of BP_{mm} monomer.

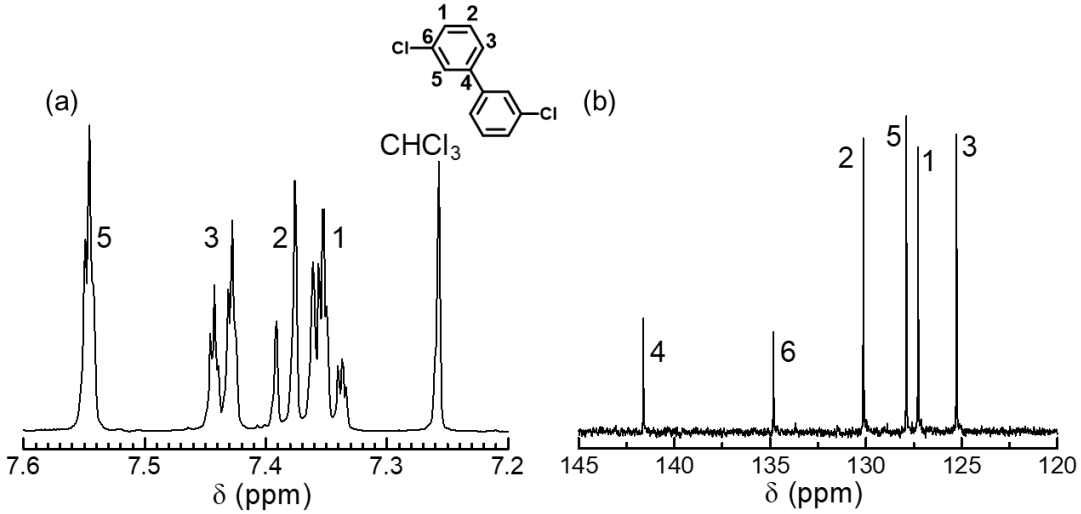

Figure 2-2 (a) ^{1}H and (b) ^{13}C NMR spectra of BP_{mm} monomer in $CDCl_3$ at r.t.

2.2.5 Synthesis of SPP-QP and SPP-BP

SPP-QP was synthesized according to the literature [12]. A typical synthetic procedure for SPP-BP is as follows (target ion exchange capacity, IEC_{target} = 3.1 mequiv. g^{-1}, *m*-/*p*-ratio = 4/1). A 100-mL three-neck flask equipped with a magnetic stirring bar and nitrogen inlet/outlet was charged with BP_{mm} monomer (4.48 mmol, 1.00 g), BP_{pp} monomer (1.12 mmol, 0.250 g), SP monomer (5.12 mmol, 1.16 g), 2,2'-bipyridine (33.8 mmol, 5.28 g), K_2CO_3 (5.63 mmol, 0.778 g), DMSO (62.5 mmol), and toluene (10 mL). After the azeotropic removal of water at 170 ºC for 2 h with a dean-stark trap, the reaction mixture was cooled to 80 ºC followed by the addition of $Ni(cod)_2$ (32.2 mmol, 8.85 g). The polymerization reaction was carried out at 80 ºC for 3 h, and then the reaction mixture was poured into a large excess of methanol. The crude product was washed with 6 M hydrochloric acid and water repeatedly. The obtained polymer was dried in a vacuum oven at 60 ºC for overnight (82.6 %).

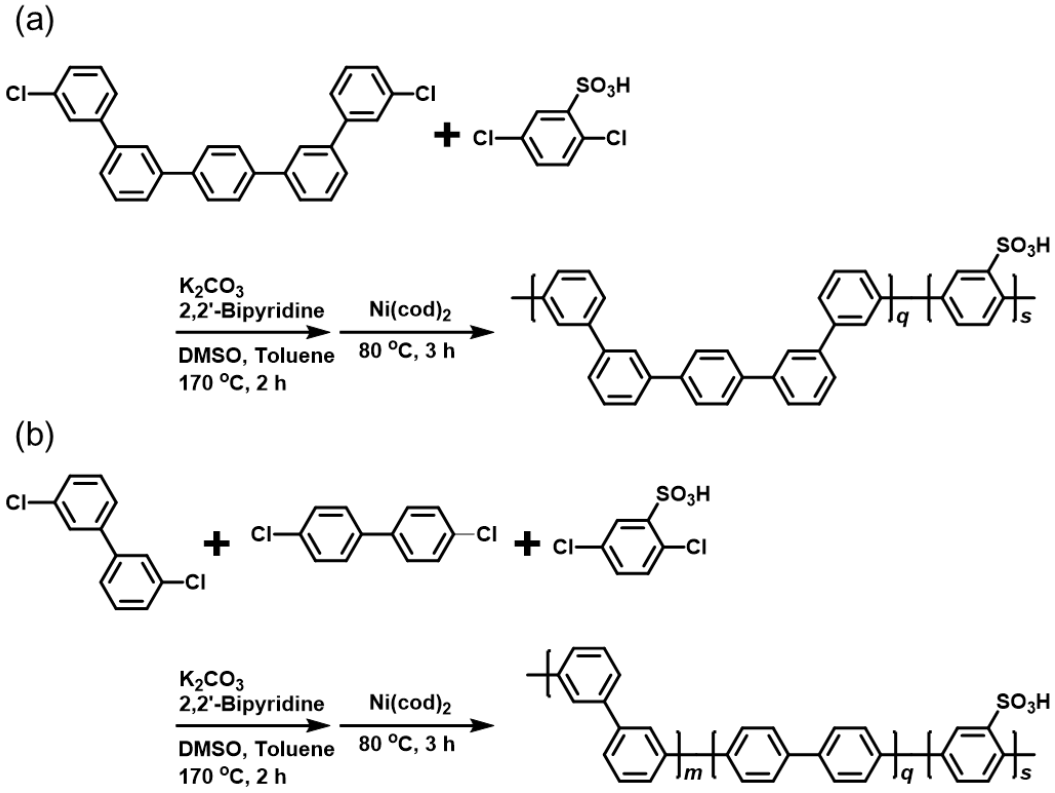

Scheme 2-4 Synthesis of the (a) SPP-QP and (b) SPP-BP.

2.2.6 Synthesis of SPP-MP

A typical synthetic procedure for SPP-MP is as follows (target ion exchange capacity, IEC_{target} = 3.1 mequiv. g^{-1}, *m*-/*p*- ratio = 4/1). A three-neck round bottom flask equipped with a magnetic stirring bar and a nitrogen inlet/outlet was charged with sodium 2,5-dichlorobenzenesulfonate ($SP\text{-}Na^+$) monomer (9.48 mmol, 2.36 g), 2,2'-bipyridine (38.2 mmol, 5.96 g), DMSO (20mL), and toluene dehydrate (10 ml). After azeotropic removal of water at 170 °C for 2 h with a Dean-Stark trap, the reaction mixture was cooled to 80 °C followed by the addition of *m*-dichlorobenzene (8.33 mmol, 1.22 g), *p*-dichlorobenzene (2.08 mmol, 0.31 g), and $Ni(cod)_2$ (18.2 mmol, 5.00 g). The polymerization reaction was carried out at 80 °C for 2 h, and then the reaction mixture was poured into a large excess of methanol to precipitate the product. The crude product was washed with 6 M hydrochloric acid and water repeatedly. Drying in vacuum at 105 °C yielded the target SPP-MP terpolymer in 92% yield (2.09 g).

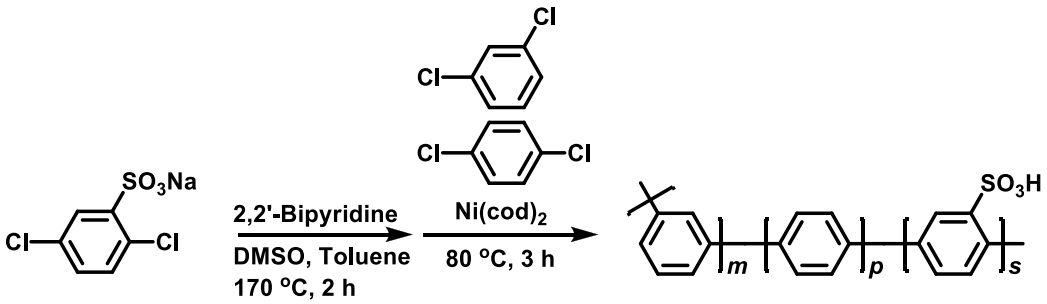

Scheme 2-5 Synthesis of the SPP-MP.

2.2.7 Membrane preparation

The SPP-QP, SPP-BP, or SPP-MP (0.49 g) was dissolved in 5 mL of DMSO and cast onto a flat glass plate. The solution was dried at 60 °C to obtain a thin membrane. The membrane was further dried under reduced pressure at 80 °C for at least 3 h. Then, the membrane was immersed in 1 M sulfuric acid overnight, washed with water several times, and dried at room temperature.

2.3 Results and discussion

2.3.1 The effect of the hydrophobic composition on polyphenylene ionomer synthesis

In our previous report, we demonstrated that the sulfonated polyphenylene ionomer membrane with *m*-/*p*- = 4/1 for hydrophobic component (QP monomer, -*m*-*m*-*p*-*m*-*m*- linkages) was highly soluble in polar aprotic solvent, resulted in flexible and high-performing PEMs. However, there still be unclear whether the *m*-/*p*- = 4/1 for hydrophobic component would be the best hydrophobic composition. Further, as discussed above, the QP monomer needs two consecutive synthetic steps, which may reduce the cost effectiveness. Thus, by using lower-cost hydrophobic monomers (Biphenylene monomer, BP_{mm}: -*m*-*m*-, BP_{pp}: -*p*-*p*-), the influence of the composition in the hydrophobic component on polyphenylene ionomer synthesis was investigated.

The copolymerization reaction of SPP-BP was conducted using bis(1,5-cyclooctadiene) nickel(0) ($Ni(cod)_2$) as a mediator, 2,2'-bipyridine as a ligand, and BP_{mm}, BP_{pp}, SP as comonomers to obtain the SPP-BP. The monomers were readily available; i.e., BP_{mm} and BP_{pp} were successfully synthesized from commercially available reagents in one step reaction, and SP was commercially available. Table 2-1 summarizes the effect of the composition in the hydrophobic component (i.e., *m*/*p* ratio) on solubility, molecular weight, and membrane forming capability of the polymers. In all cases, the (*m*+*p*)/*s* ratios were set to be the same (ca. 1.09) so that the copolymers contained the same concentration of the sulfonic acid groups or ion exchange capacity (IEC_{target} = ca. 3.1 mequiv. g^{-1}). Consequently, the solubility of the copolymers increased with increasing the *m* content (i.e., BP_{mm}), and the SPP-BP with *m*/*p* ratio higher than 1 (runs 4-6) dissolved completely in polar aprotic solvents such as DMSO or DMF. It is well-known that unsubstituted

poly(*p*-phenylene)s have very low solubility because of the strong interpolymer interaction caused by its high linearity and planarity. Among the SPP-BP tested, only SPP-BP (run 4) provided thin, bendable membrane. As we discussed in our previous paper [12], the l_p of polyphenylenes became smaller than 0.7 nm when the *m*-phenylene/*p*-phenylene ratio was higher than 4/1. The l_p values were similar to those of the common flexible polymers such as polyethylene (l_p = ca. 0.7 nm) [13], indicating that such kinked conformations or flexible coils enabled inter-polymer entanglement resulting in the formation of tough, flexible SPP-BP (run 4) and SPP-QP membranes. SPP-BP (runs 5 and 6), however, did not provide self-standing membranes most probably because of insufficient molecular weight (Table 2-1). Comparison of ^{1}H NMR spectra (Figure 2-3) enabled approximate assignment of SPP-BP.

Table 2-1 IEC, molecular weight, and properties of SPP-BP with various compositions, and of SPP-MP, SPP-QP.

Run	Composition[a]			IEC (mequiv. g^{-1})			Molecular weight (kDa)[b]		Yield (%)	Solubility[c]	Membrane forming capacity
	m	*p*	*s*	Feed	NMR	Titration	M_n	M_w			
1	0.00	1.09	1.00	3.1	3.8[d]	-	16.8[d]	119.6[d]	85	×	-
2	0.12	0.97	1.00	3.1	3.5[d]	-	25.3[d]	114.7[d]	95	×	-
3	0.55	0.55	1.00	3.1	2.8[d]	-	35.2[d]	137.9[d]	98	×	-
4	0.88	0.22	1.00	3.1	2.4	2.4	36.6	136.4	94	○	○
5	0.97	0.12	1.00	3.1	2.5	-	28.0	95.6	88	○	×
6	1.09	0.00	1.00	3.1	2.2	-	23.1	74.4	94	○	×
SPP-MP	1.75	0.44	1.00	3.1	2.9	2.5	12.9	98.8	92	○	○
SPP-QP	-[e]			3.1	2.6	2.4	27.6	120.4	97	○	○

[a] Calculated from feed monomer ratio. [b] Determined by GPC. [c] In DMSO or DMF. [d] Soluble parts. [e] Similar composition with SPP-BP (run 4).

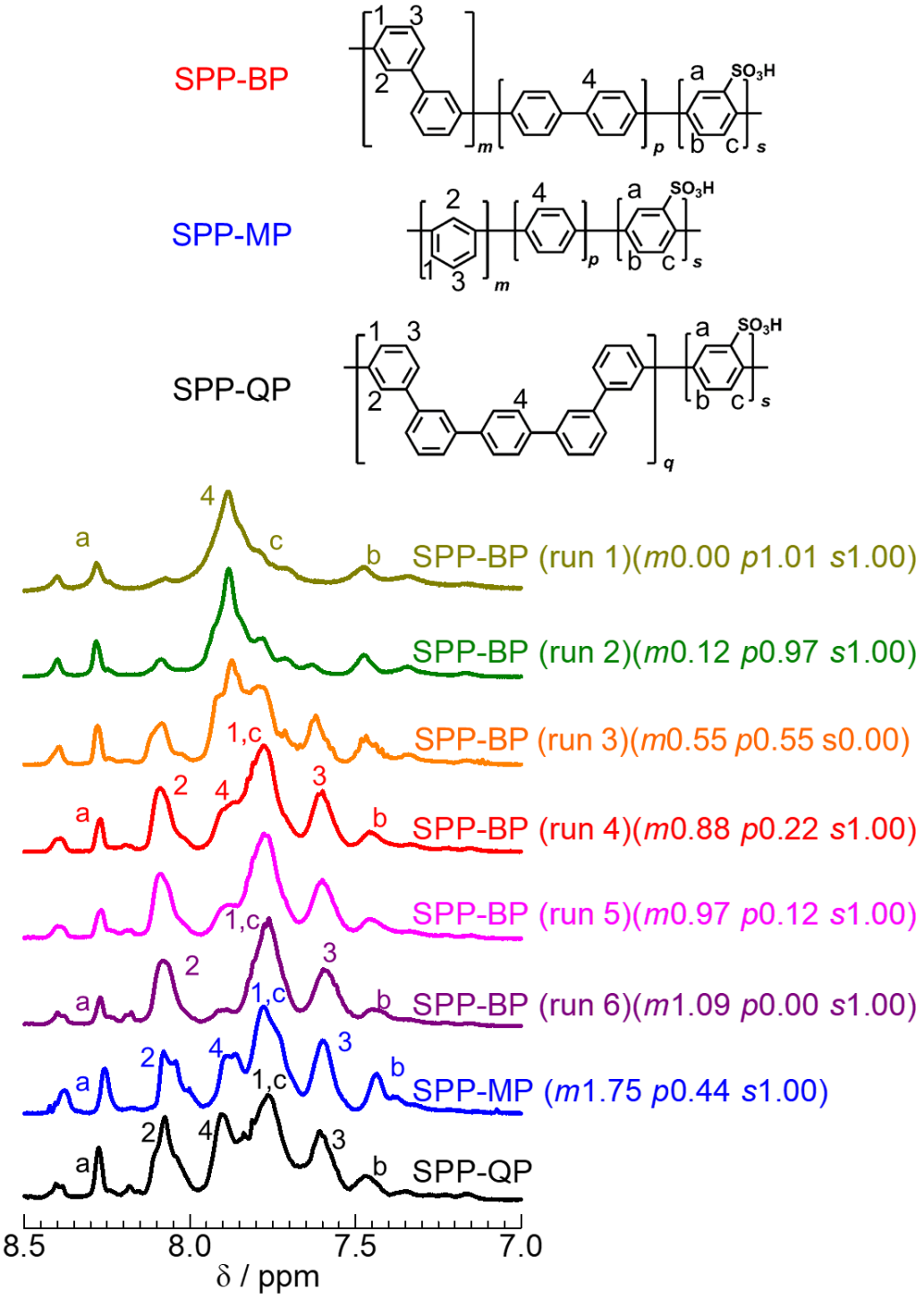

Figure 2-3 ^{1}H NMR spectra of SPP-BP with various compositions, SPP-MP, and SPP-QP in DMSO-d_6 at 80 °C.

In the above SPP-BP and SPP-QP studies, it was found that, for the hydrophobic composition of the polyphenylene ionomer, *m*-/*p*- = 4/1 universally seemed to be the best composition. Thus, SPP-MP with *m*-/*p*- = 4/1 for hydrophobic component and IEC = 2.5 (i.e., to be the same unsubstituted *meta*-phenylene / unsubstituted *para*-phenylene / sulfonated *para*-phenylene ratio for the SPP-MP, SPP-BP, and SPP-QP) was synthesized under similar synthetic conditions. Note that, only in the SPP-MP synthesis, the hydrophobic monomers (*m*-dichlorobenzene and *p*-dichlorobenzene) were added at 80 °C after the azeotropic dehydration process (at 170 °C) due to the low boiling points of *m*-dichlorobenzene (173 °C) and *p*-dichlorobenzene (174 °C). The resulting SPP-MP (see Table 2-1) showed high solubility (soluble in polar aprotic solvents such as DMAc, DMSO, and NMP), which was similar with that of SPP-QP. Casting from DMSO solution provided brown, transparent, and bendable SPP-MP membrane. The molecular weight estimated from GPC was in the order SPP-BP (M_n = 25.6 kDa, M_w = 114.1 kDa) > SPP-MP (M_n = 12.9 kDa, M_w = 98.8 kDa) > SPP-QP (M_n = 7.3 kDa, M_w = 74.9 kDa), suggesting that the size of the hydrophobic monomers was not relevant. The IEC values (IEC = 2.5 mequiv. g^{-1}) determined by titration were comparable to that of SPP-BP or SPP-QP, suggesting a successful copolymerization reaction.

As shown in Figure 2-3, the ^{1}H NMR spectra were very similar because of the similar composition (unsubstituted *m*-phenylene/unsubstituted *p*-phenylene/sulfonated *p*-phenylene ratio). One of the noticeable differences was observed at around 7.9 ppm, assigned to protons ***4*** in unsubstituted *para*-phenylene connected with the unsubstituted *meta*-phenylene. The signal intensity at around 7.9 ppm was in the order SPP-QP > SPP-MP > SPP-BP, suggesting that this sequence (i.e., unsubstituted *para*-phenylene and unsubstituted *meta*-phenylene) was most contained in SPP-QP. This is reasonable because

the unsubstituted *para*-phenylene in SPP-QP is connected solely with the unsubstituted *meta*-phenylene, while all components (unsubstituted *meta*-phenylene, unsubstituted *para*-phenylene, and sulfonated *para*-phenylene) can be connected with each other for SPP-BP and SPP-MP. The protons ***4*** must be in different environments resulting in a broader, less prominent peak.

Figure 2-4 Photo images of SPP-MP, SPP-BP (run 4), and SPP-QP membranes.

2.3.2 Connectivity of unsubstituted and sulfonated phenylene rings

To estimate the molecular sequence of SPP-MP, SPP-BP (run 4), and SPP-QP, numerical calculation was conducted on Mathematica (Figure 4-5). Specifically, ratio of each bond (SP-SP linkage, etc) in the main chain, and continuity of each phenylene ring (or randomness) were estimated by numerically averaging 1,000,000 polymer chains (or 1,000,000 molecular sequences) randomly generated. Note that each polymer chain was set to have IEC of 2.37 meq g^{-1} and molecular weight of ca. 42 kDa (i.e., number of unsubstituted *m*-, *p*-phenylene, and SP rings were 280, 70, and 100, respectively), which simulated the SPP-MP, SPP-BP (run 4), and SPP-QP. The simulated SPP-BP (run 4) had much higher ratio of unsubstituted *p*-Ph-unsubstituted *p*-Ph linkages (ca. 8.76%) than that

of SPP-MP (ca. 4.90%) and SPP-QP (ca. 0%) due to the monomer structure (i.e., BP_{pp}) rather than the molecular sequence. This difference in the molecular sequence in SPP-MP, SPP-BP (run 4), and SPP-QP must cause differences in electronic state, local conformation, self-assembling behavior of the copolymers. In fact, the color of SPP-BP (run 4) membrane was much darker than that of SPP-MP and SPP-QP (Figure 2-4). This result is reasonable taking into account much higher continuity of the unsubstituted *p*-phenylene groups in SPP-BP (run 4) than that in SPP-MP and SPP-QP. More importantly, the ratio of SP-SP linkage (ca. 4.90%) in SPP-MP (run 4) was lowest in that of SPP-BP (ca. 8.02%) and SPP-QP (ca. 12.97%). Similarly, the ratio of unsubstituted Ph-unsubstituted Ph linkage (ca. 60.49%) in SPP-MP (run 4) was also lowest in that SPP-BP (ca. 63.64%) of SPP-QP (ca. 68.69%). Both the unsubstituted Ph and SP rings in SPP-MP (run 4) were estimated to be in each segment with lower number of continuous rings than that of SPP-BP or SPP-QP. In other words, SPP-MP was likely to contain shorter sequenced lengths of hydrophilic and hydrophobic components than those in SPP-BP and SPP-QP.

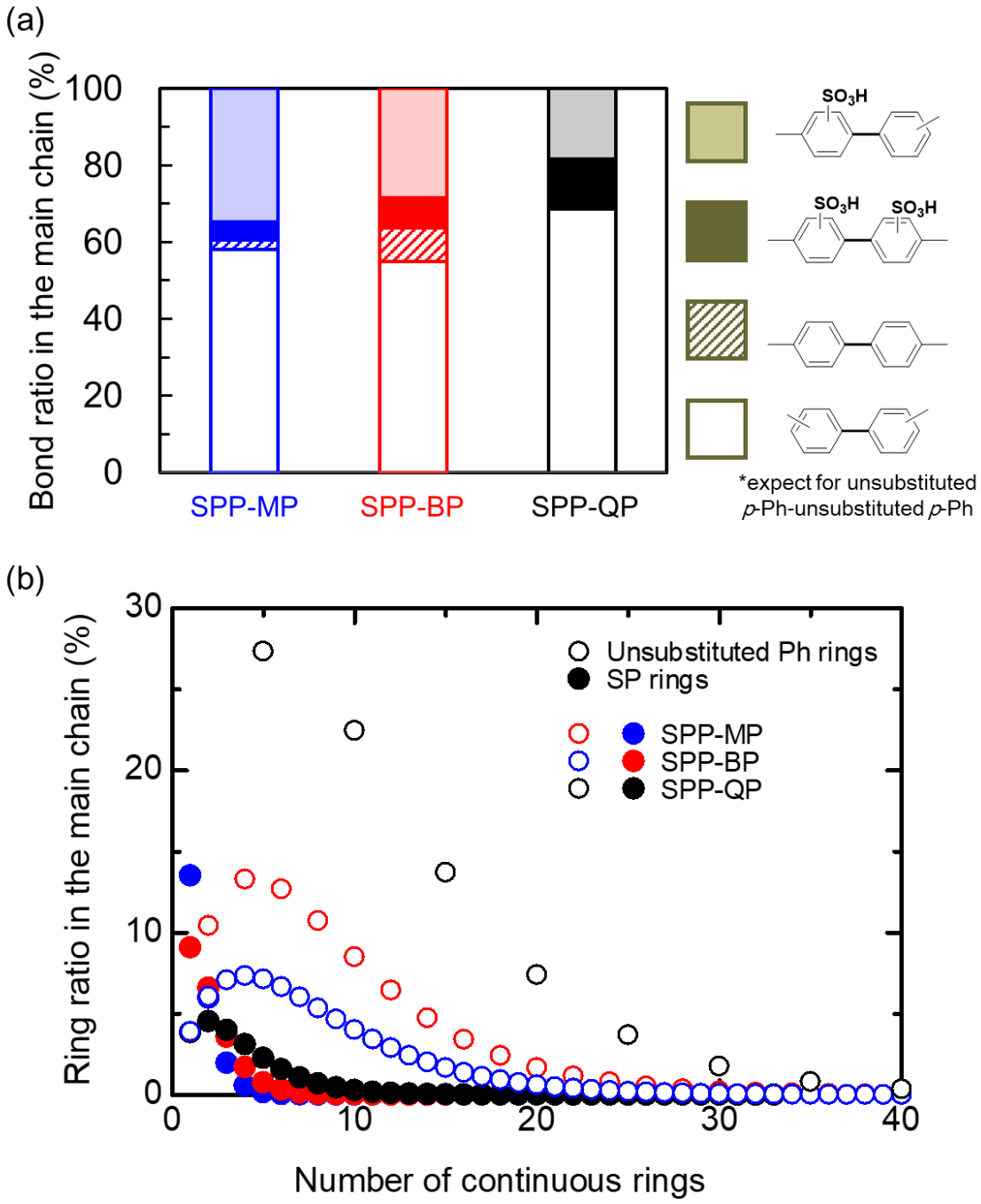

Figure 2-5 The ratios of (a) each bond and (b) each phenylene ring were estimated by numerically averaging 1,000,000 polymer chains randomly generated. Each polymer chain was set to have IEC (2.37 mequiv. g^{-1}) and molecular weight (ca. 42 kDa, number of unsubstituted *m*-, *p*-Ph, and SP rings were 280, 70, and 100, respectively), which simulated the SPP-MP, SPP-BP (run 4), and SPP-QP. The calculation was performed with Mathematica.

2.3.3 Randomness of hydrophilic component

Another difference was observed in the integral ratio of the three signals at around 8.0-8.5 ppm correlated with the protons ***a*** in the sulfonated *para*-phenylene (SP). Previously, we assigned the three peaks of protons ***a***, as "unsubstituted phenylene - *SP* (***a*₁**) - unsubstituted phenylene", "SP - *SP* (***a*₂**) - unsubstituted phenylene", and "SP - *SP* (***a*₃**) - SP" (Figure 2-6), and defined the integral ratio of (***a*₁**/***a*₁**+***a*₂**+***a*₃**) as the randomness of the SP unit or the isolated hydrophilic component (SP) ratio in the backbone for SPP-QP prepared with different polymerization promoters (Note that peaks ***a*₃** and ***2*** were overlapping) [(14)]. The ratio of ***a*₃** was calculated using the following equation:

$$\boldsymbol{a_3} = I - NX - 2Y - \boldsymbol{a_1} - \boldsymbol{a_2} \quad (2\text{-}1)$$

where *I* is the total and ***a*₁**, ***a*₂** and ***a*₃** are the integral values estimated from the ^{1}H NMR spectra, *N* is the number of protons in the hydrophobic components, and *X* and *Y* are the compositions of hydrophilic and hydrophobic segments calculated from the titrated IEC values. The randomness of the SP unit was calculated using the titrated IEC values and was in the order, SPP-MP (51%) > SPP-BP (32%) > SPP-QP (19%), indicating that the hydrophobic components dominated the sequence of the hydrophilic component.

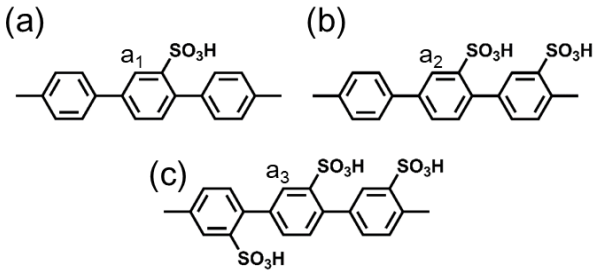

Figure 2-6 Possible sequences of the SP units.

2.4 Conclusion

In conclusion, the polyphenylene ionomers (SPP-MP and SPP-BP) were designed and synthesized via a simple, cost-effective, practical approach. In this chapter, two factors were focused, the effect of composition of hydrophobic monomers on the membrane forming capability and influence of the sequence length of hydrophobic monomer on randomness of hydrophilic unit. The increasing *p*-phenylene content lead large molecular weight enough to form membranes. On the other hand, the solubility of the copolymers decreased with increasing the *p*-phenylene content, and the SPP-BP with *m*/*p* ratio lower than 1 was only partially soluble in polar aprotic solvents. Among the SPP-BP tested, only SPP-BP with *m*/*p* = 4/1 provided thin, bendable membrane, indicating that the persistence length has large impact on the membrane forming capability. The sequence length of the hydrophobic components affected much on the polymer configuration. The most remarkable difference among the three membranes was the randomness of sulfonated phenylene (SP) unit calculated from ^{1}H NMR spectra and titration IEC values. The randomness of SP unit was in the order of SPP-MP (51%) > SPP-BP (32%) > SPP-QP (19%), indicating that the hydrophobic components altered the sequence of the hydrophilic component.

2.5 Reference

(1) Kreuer, K.-D. *Chem. Mater.* **2014**, *26*, 361-380.

(2) Hickner, M. A. *Mater. Today* **2010**, *13*, 34-41.

(3) Wang, Y.; Chen, K. S.; Mishler, J.; Cho, S. C.; Adroher, X. C. *Appl. Energy* **2011**, *88*, 981-1007.

(4) Kusoglu, A.; Weber, A. Z. *Chem. Rev.* **2017**, *117*, 987-1104.

(5) Rikukawa, M.; Sanui, K. *Prog. Polym. Sci.* **2000**, *25*, 1463-1502.

(6) Hickner, M. A.; Ghassemi, H.; Kim, Y. S.; Einsla, B. R.; McGrath, J. E. *Chem. Rev.* **2004**, *104*, 4587-4612.

(7) Miyatake, K.; Zhou, H.; Uchida, H.; Watanabe, M. *Chem. Commun.* **2003**, 368-369.

(8) Miyake, J.; Watanabe, M.; Miyatake, K. *ACS Appl. Mater. Interfaces* **2013**, *5*, 5903-5907.

(9) Zhang, Y.; Miyake, J.; Akiyama, R.; Shimizu, R.; Miyatake, K. *ACS Appl. Energy Mater.* **2018**, *1*, 1008-1015.

(10) Skalski, T. J. G.; Britton, B.; Peckham, T. J.; Holdcroft, S. *J. Am. Chem. Soc.* **2015**, *137*, 12223-12226.

(11) Adamski, M.; Skalski, T. J. G.; Britton, B.; Peckham, T. J.; Metzler, L.; Holdcroft, S. *Angew. Chem. Int. Ed.* **2017**, *56*, 9058-9061.

(12) Miyake, J.; Taki, R.; Mochizuki, T.; Shimizu, R.; Akiyama, R.; Uchida, M.; Miyatake, K. *Sci. Adv.* **2017**, *3*, eaao0476.

(13) Kuei, B.; Gomez, E. D. *Soft Matter* **2017**, *13*, 49-67.

(14) Hosaka, I.; Sawano, T.; Kimura, T.; Matsumoto, A.; Miyake, J.; Miyatake, K. *Bull. Chem. Soc. Jpn.* **2020**, *93*, 393-398.

Chapter 3 Sulfonated Polyphenylenes: Structure-Property Relationships

3.1 Introduction

Recently, sulfonated polyphenylene (SPP) membranes have been one of the most promising alternatives to the current state-of-the-art perfluorinated PEM (such as Nafion) for fuel cell applications. For example, Kim *et al.* reported that an SPP membrane with pendant benzophenone and sulfonyl imide acid groups with an IEC of 1.76 mequiv. g^{-1} showed high proton conductivity (ca. 142.85 mS cm^{-1} at 90 °C and 90% relative humidity (RH)) and was durable against free radical attack [(1)]. A completely heteroatom linkage-free ionomer membrane was reported by Holdcroft *et al.* Its SPP membrane with six pendant phenyl groups (IEC = 3.47 mequiv. g^{-1}) showed high proton conductivity (338 mS cm^{-1} at 80 °C and 95% RH) [(2)]. We have developed a simpler version of the SPP ionomer (SPP-QP) composed of *m*- and *p*-phenylene groups with sulfonic acid substituents [(3)]. The SPP-QP membrane exhibited high proton conductivity. High stability was further verified using an open-circuit voltage (OCV) hold test in a fuel cell. The initial OCV for the SPP-QP membrane with IEC = 2.4 mequiv. g^{-1} was 1.04 V at 80 °C and 30% RH, which was retained after 1,000 hours (decay rate = 226 μV $hour^{-1}$).

In Chapter 2, I found the novel, cost-effective synthetic pathway for the SPPs. Therein, I revealed that the hydrophobic monomer size (monophenylene for SPP-MP; biphenylene for SPP-BP; and quinquephenylene for SPP-QP) significantly affect the molecular structure (i.e., randomness of hydrophilic unit) of the SPPs. The molecular structure must affect the self-assembling structures as well as membrane properties.

In this Chapter, I disclose in detail the effect of the hydrophobic comonomers (monophenylene for SPP-MP; biphenylene for SPP-BP; and quinquephenylene for SPP-QP) on the structure, morphology, and properties of SPP ionomer membranes. For effective comparison, the *m*-/*p*-phenylene ratio was set at the same value, 4/1, while their sequence was differed by the use of different hydrophobic comonomers (monophenylene, -MP; biphenylene -BP; and quinquephenylene, -QP, respectively). The structure and morphology was analyzed via nuclear magnetic resonance (NMR) spectroscopy, transmission electron microscopy (TEM) images, small-angle X-ray scattering (SAXS), and small-angle neutron scattering (SANS) measurements. These results are discussed quantitatively in relation to relevant membrane properties such as water affinity, proton conductivity, and mechanical strength.

3.2 Experimental

3.2.1 Morphology

3.2.1.1 Transmission Electron Microscope (TEM) observation

For TEM observation, membrane sample was stained in 0.5 M lead (II) acetate aqueous solution, washed with ultrapure water, and dried. The stained membrane sample was embedded in epoxy resin, sectioned to 50 nm thickness with a Leica microtome Ultracut UCT, and placed on a copper grid. Images were taken on a Hitachi H-9500 TEM with an accelerating voltage of 200 kV.

3.2.1.2 Small-Angle X-lay Scattering (SAXS)

SAXS experiment was conducted with a Rigaku NANO-Viewer diffractometer equipped with a temperature/humidity-controllable chamber. The membrane (ca. 150 μm)

was equilibrated for at least 2 h under the tested conditions.

3.2.1.3 Small-Angle Neutron Scattering (SANS)

SANS experiments were conducted at beam-line 15, TAIKAN [4], MLF, J-PARC, which is equipped with a temperature/humidity-controllable chamber. The SANS curves were obtained in the q-range of 0.05 - 170 nm^{-1}. The q term, the scattering vector, is given by $q = 4\pi\sin(\theta/2)/\lambda$, where θ is the scattering angle and λ is the neutron wavelength. The samples were mounted on a sample cell, which was a flat-type cell with quartz windows and a titanium spacer, sealed by back-up O-rings and tightening retainers on both sides. D_2O was used for the humidification. The membranes were equilibrated under the given temperatures and humidities for at least 30 min prior to the measurement. The measurement was done for 3 h for each condition. The hydrophilic domain size (ξ) and the distance between the hydrophilic domains (D) were calculated using the power law and the Teubner-Strey (TS) model [5, 6].

3.2.2 Water uptake and proton conductivity

The liquid water uptake was measured gravimetrically and volumetrically. The weight and volume of dry membranes was measured after drying under reduced pressure at 40 ^oC for 12 h. Then, the membranes were immersed in distilled water at 40 ^oC for 1 h. The hydrated membranes were taken out from water. After removal of excess water, the weight and volume of hydrated membranes was measured. The gravimetrical change was calculated from the following equation: $(W_{wet} - W_{dry}) / W_{dry} \times 100\%$, where W_{wet} was the weight of the wet membrane and W_{dry} was the weight of the dry membrane, and the volumetrically changes was calculated from as follows: $(V_{wet} - V_{dry}) / V_{dry} \times 100\%$, where

V_{wet} was the volume of the wet membrane and V_{dry} was the volume of the dry membrane. Water uptake and proton conductivity of the membranes from vaper phase were measured simultaneously at 80 ºC with a solid electrolyte analyzer system (MSBAD-V-FC, Bel Japan Co.) equipped with a temperature/humidity-controllable chamber. Weight of the membranes was measured with a magnetic suspension balance at a given humidity, and the water uptake was calculated using the following equation: (weight of hydrated membrane – weight of dry membrane) / weight of dry membrane × 100. Drying at 80 ºC for 3 h under reduced pressure gave the weight of dry membrane, and exposure to a given humidity for at least 2 h gave the weight of hydrated membrane. Proton conductivity was measured with a four probe conductivity cell equipped with a Solartron 1255B and SI 1287 impedance analyzers in the same chamber. Ion conducting resistances (R) were determined from the impedance plot obtained in the frequency range from 1 to 105 Hz. The proton conductivity (σ) was calculated from the equation: $\sigma = l / (A \times R)$, where A and l are the conducting area and the electrode distance, respectively.

3.2.3 Mechanical strength

Stress-strain curves were obtained by a Shimadzu AGS-J 500N universal test machine attached with a Toshin Kogyo Bethel-3A temperature/humidity-controllable chamber. The membrane sample was cut into a dumbbell shape (DIN-53504-S3, 35 × 6 mm (total) and 12 × 2 mm (test area)). The measurement was carried out at 80 ºC and 60% RH at a tensile rate of 10 mm min^{-1}.

3.3 Result and discussion

3.3.1 Morphology

3.3.1.1 TEM observation

TEM images were obtained to reveal the effect of the sequence (randomness) of the hydrophilic components on the membrane morphology under dry conditions. Figure 3-1 shows the cross-sectional TEM images of the SPP-MP, SPP-BP, and SPP-QP membranes stained with Pb^{2+} ions, in which the dark areas represent the hydrophilic clusters composed of lead-stained sulfonic acid groups and the bright areas represent the hydrophobic clusters. It is seen from the TEM images that the membranes showed a typical phase-separated morphology based on the hydrophilic/hydrophobic differences in the components, although the interfaces of the domains were not very distinct due to the rigid polyphenylene structure. The size of the clusters was in the order, SPP-MP (ca. 1.8 ± 0.4 nm) = SPP-BP (ca. 1.8 ± 0.3 nm) [(7)] < SPP-QP (ca. 2.8 ± 0.2 nm) [(3)] for hydrophilic component and SPP-MP (ca. 1.9 ± 0.4 nm) = SPP-BP (ca. 2.0 ± 0.5 nm) < SPP-QP (ca. 2.7 ± 0.8 nm) for hydrophobic component, respectively. The result seems reasonable because the higher randomness should lead to a smaller sequence of the hydrophilic component. As the randomness increased, more isolated SP units must have been included, suppressing the self-aggregation of the components.

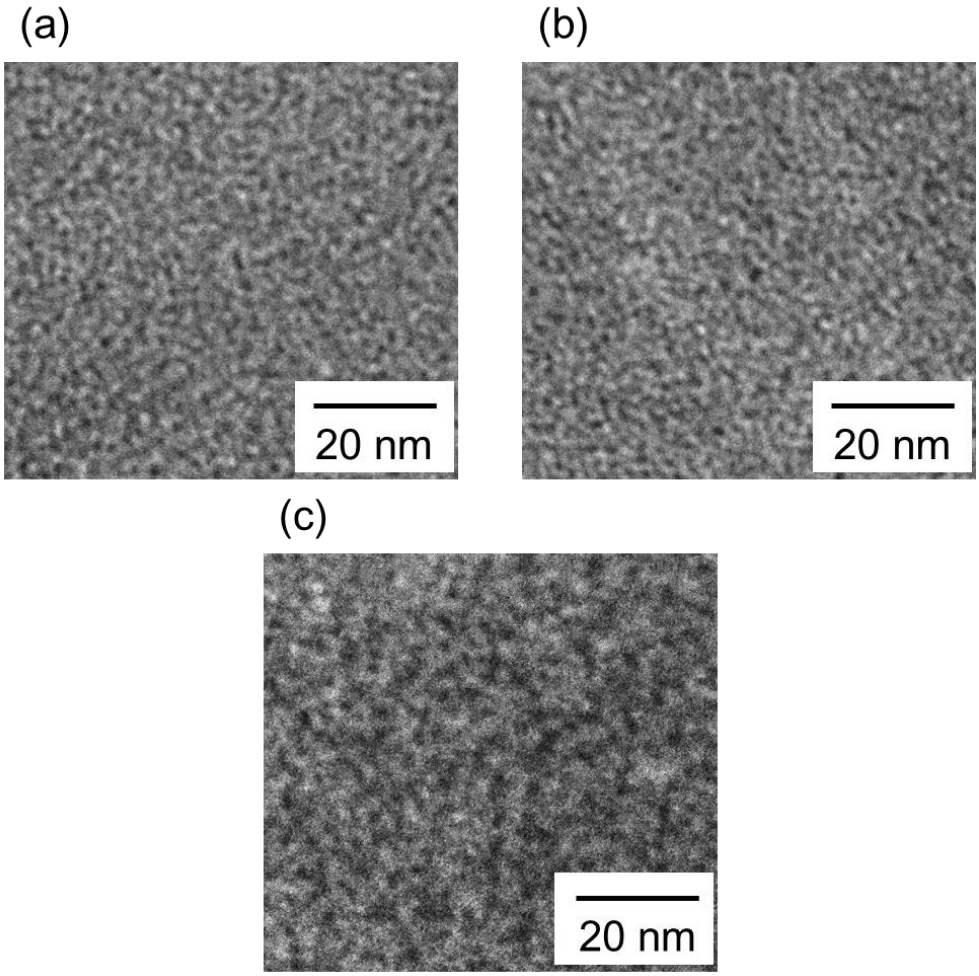

Figure 3-1 TEM images of (a) SPP-MP (IEC = 2.5 mequiv. g^{-1}), (b) SPP-BP (IEC = 2.4 mequiv. g^{-1}), and (c) SPP-QP (IEC = 2.4 mequiv. g^{-1}) membranes stained with Pb^{2+} ions.

3.3.1.2 SAXS measurement

To gain morphological information under more practical conditions, SAXS measurements were carried out at 80 °C and at various humidities. Figure 3-2 shows the scattered intensity as a function of the scattering vector (q) for the three membranes. In the SAXS patterns of the SPP-MP and SPP-BP membranes, no obvious peaks were observed, and their humidity dependence was rather minor even though hydrophilic clusters were observed by TEM. This could imply that the electron density difference between the hydrophobic and hydrophilic SP domains was small because the higher randomness of the hydrophilic component must have suppressed the self-aggregation of the sulfonic groups. In contrast, an SPP-QP membrane with a lower randomness showed a broad but an obvious peak at q = ca. 0.78 nm^{-1} or at ca. 8.0 nm of the d spacing at 30% RH, which became smaller with the increasing humidity. The results suggest that absorbed water was located not only in the hydrophilic domains but also to some extent in the hydrophobic ones, resulting in the randomization of the phase-separated morphology, as discussed in our previous paper [8]. As a result, filling the hydrophilic domains with water must have decreased the scattering intensity.

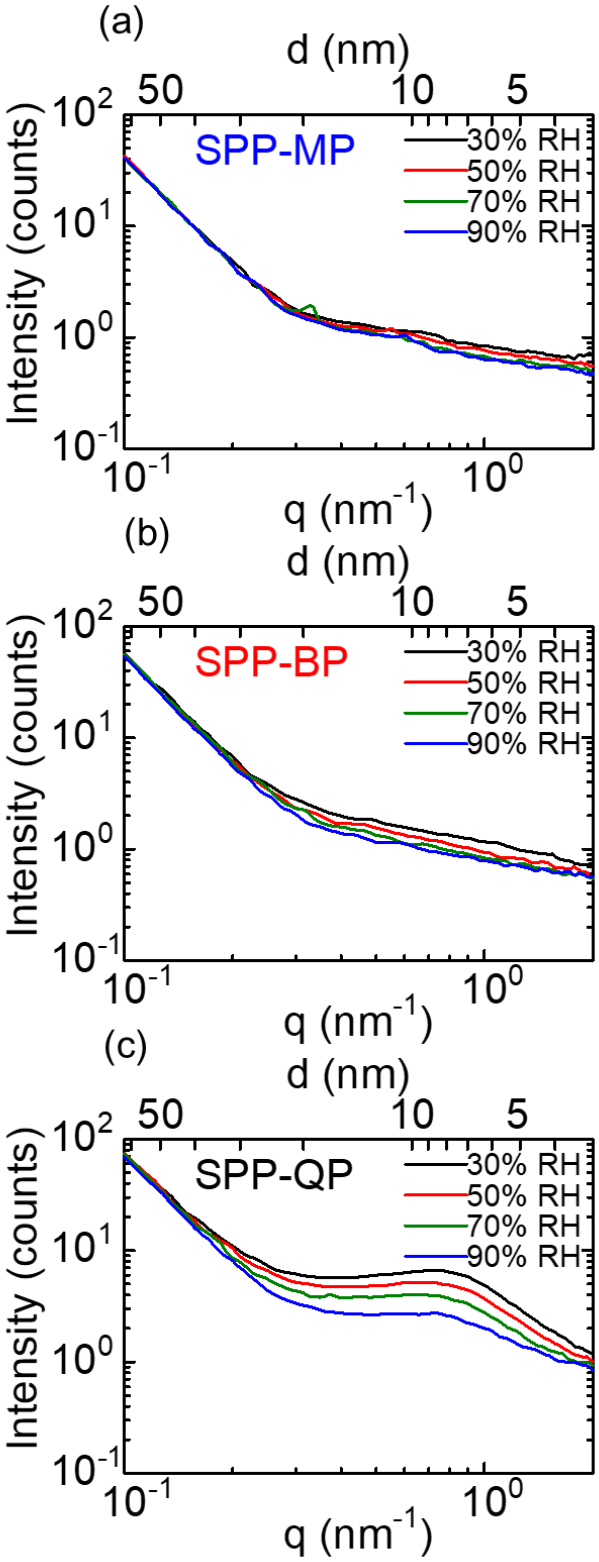

Figure 3-2 SAXS patterns of (a) SPP-MP, (b) SPP-BP, and (c) SPP-QP membranes at 80 °C, 30-90% RH.

3.3.1.3 SANS measurement

To further investigate the morphology of the membranes, in particular, the structure of the absorbed water molecules, SANS measurements were carried out at 80 °C under controlled humidity conditions. Deuterium has a large positive coherent scattering length, while hydrogen has a negative scattering length, and thus, hydrophilic clusters adsorbing D_2O have large contrast in comparison to the hydrophobic clusters. Figure 3-3 shows the SANS patterns of SPP-MP, SPP-BP, and SPP-QP membranes humidified with D_2O. Weak peaks were observed for SPP-BP and SPP-QP membranes, while no peaks were observed for the SPP-MP membrane under dry conditions (0% RH). As the humidity increased, the scattering intensity increased in all samples. The SANS patterns were more related with the structure of water filling in the membranes. The development of the peak (ca. q = 0.7 nm^{-1}) with humidity was the most pronounced for the SPP-QP membrane. From the background-subtracted profiles, the slopes in the Porod region were roughly estimated to be ca. -1 for SPP-MP, -2 for SPP-BP, and -3 for SPP-QP membranes at 80% RH, suggesting that water clusters were rodlike for SPP-MP, thin disklike for SPP-BP and more spherical for SPP-QP membranes. At 80% RH, the d values were 3.1, 10.4, and 9.0 nm for SPP-MP, SPP-BP, and SPP-QP membranes, respectively, suggesting that the lower randomness of the hydrophilic component led to the formation of more uniform, larger water clusters. Then, the sum of the power law and Teubner-Strey (TS) model [5, 6, 9] was applied to the curves for more quantitative analysis. The curve fitting was performed using the following equation [9],

$$I(q) = \frac{A}{q^n} + \frac{B(8D^4\pi)}{\xi[16\pi^4+8D^2\pi^2(\xi^{-2}-q^2)+D^4(\xi^{-2}+q^2)]} + C \qquad (3\text{-}1)$$

where *A*, *B* and *C* are constants of each component. The ξ and *D* terms are the domain size and interdomain distance, respectively. Figure 3-4a,b show the humidity dependence

of the ξ and D values (note that the curve fitting was not successful for the SANS patterns of SPP-MP, SPP-BP and SPP-QP at 0% RH due to the insufficient peak intensities; see Figure 3-5). It is noted that both ξ and D values showed only minor dependence on the humidity. The ξ value of SPP-QP (ca. 2.45 nm at 80% RH) was much larger than those of SPP-BP (ca. 0.88 nm at 80% RH) and SPP-MP (ca. 0.67 nm at 80% RH). This result is reasonable, because the smaller randomness of the SP unit must have led to larger water-containing hydrophilic clusters. The D value was not correlated well with the randomness and was higher for SPP-BP and SPP-QP (ca. 7.9 nm) than for SPP-MP (ca. 3.8 nm). Figure 3-4c shows the plot of ξ/D, which represents the connectivity of the water clusters, as a function of the humidity. The ξ/D values are in the order SPP-QP > SPP-MP > SPP-BP, suggesting that the hydrophilic clusters were more interconnected for the SPP-QP membrane, while those in the SPP-BP membrane were rather isolated. The connectivity was not dependent on humidity but was nearly constant in the humidity range from 30 to 80% RH. Although the existence of dead-end channels has not been well-supported by the SANS analyses, the relatively small ξ/D values are indicative of dead-end and/or isolated channels [(10)].

Taking these parameters into account, morphological models were developed for the three polyphenylene ionomer membranes, as shown in Figure 3-6. At 30% RH, the SPP-MP and SPP-BP membranes possessed a similar morphology, while the interdomain distance of the water clusters was shorter for the SPP-MP membrane. Increasing the humidity contributed to water-filling into the hydrophilic clusters and increased the number of water clusters but did not change their size, interdomain distance, or connectivity. In the SPP-QP membrane, with the smallest randomness of the SP unit, the water clusters were larger and better-connected, compared to those of the other two

membranes, and both the SAXS and SANS patterns exhibited a much higher level of correlation, supporting these results. In other words, the membrane morphology was controllable with the randomness of the hydrophilic component, without changing other factors such as the bulk concentration of the sulfonic acid groups (or IEC), which had been believed to be more influential. Further investigation is on our future agenda to verify this hypothesis.

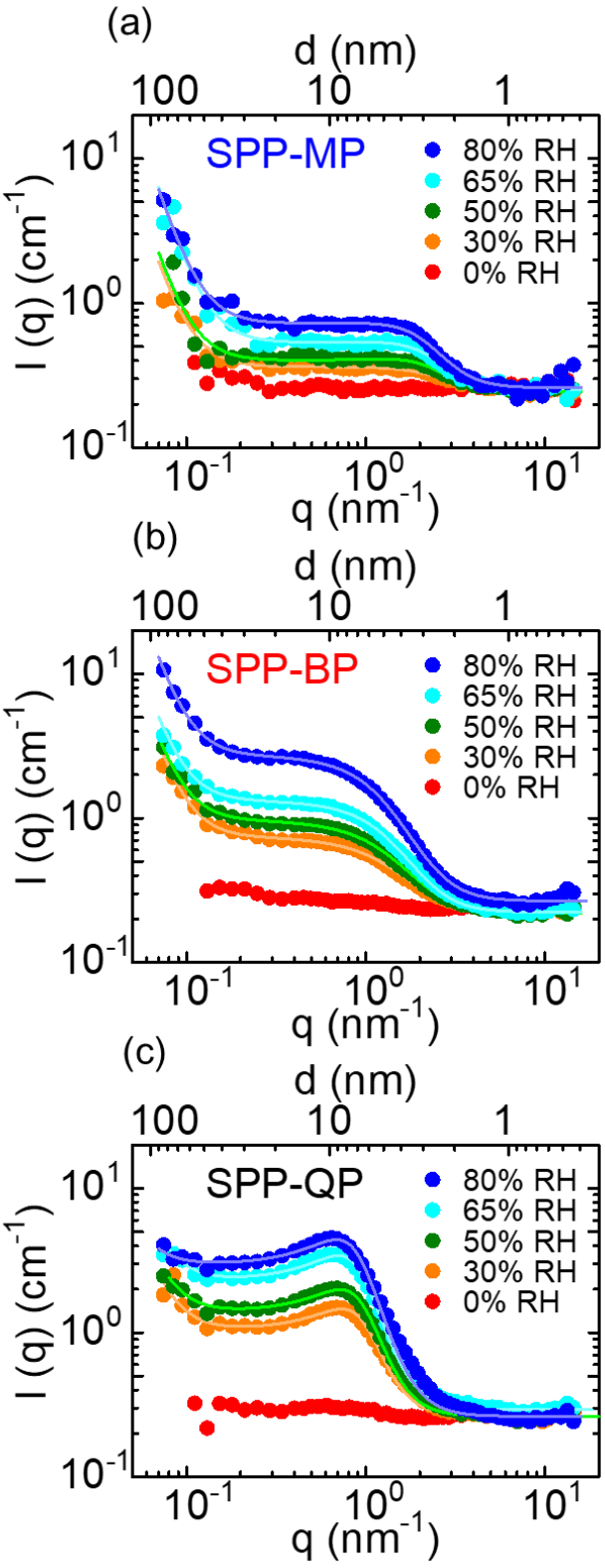

Figure 3-3 SANS patterns of (a) SPP-MP, (b) SPP-BP, and (c) SPP-QP membranes at 80 °C, 0-80% RH (D_2O). Solid lines are fitted results using eq (3-1).

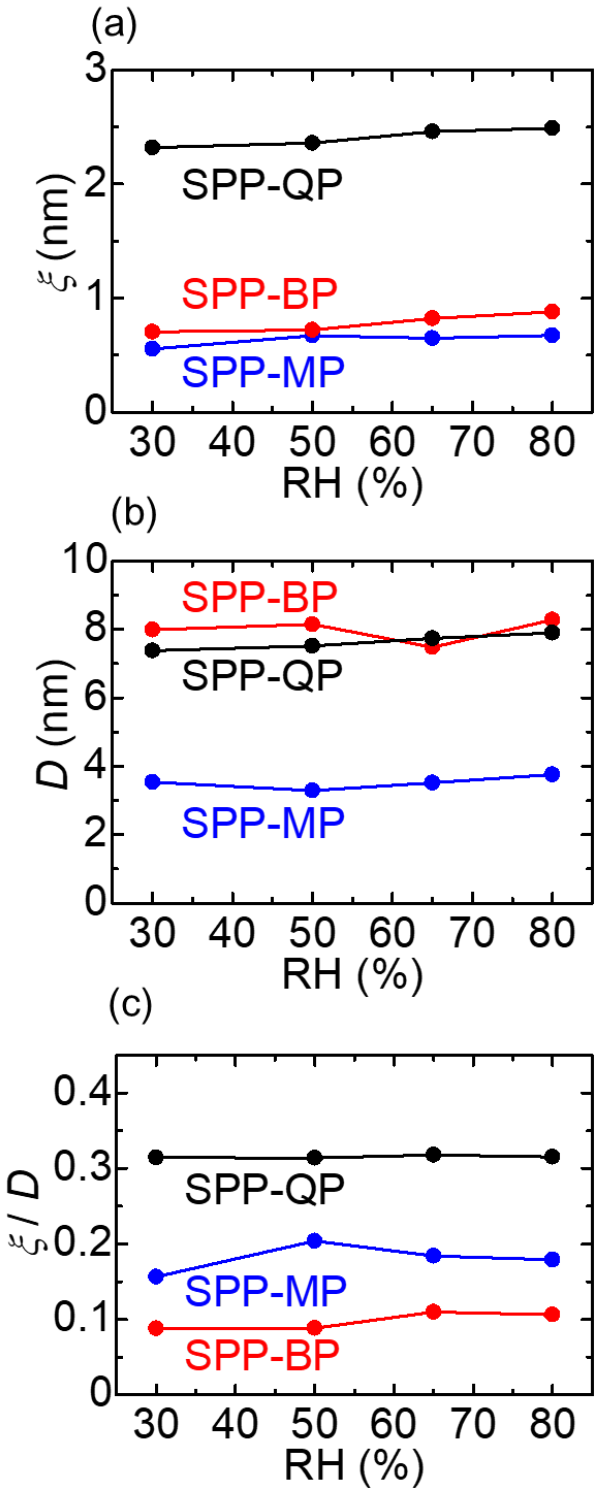

Figure 3-4 Humidity dependence of (a) domain size (ξ), (b) interdomain distance (D) and (c) ξ/D values of SPP-MP, SPP-BP, and SPP-QP membranes calculated from the SANS patterns in Figure 3-3.

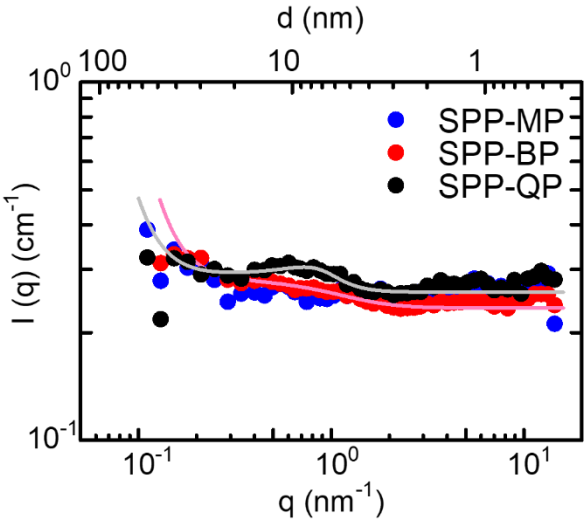

Figure 3-5 SANS patterns of SPP-MP, SPP-BP, and SPP-QP membranes at 80 °C, 0% RH (D_2O). Solid lines for SPP-BP and SPP-QP are fitted results using Eq. (3-1).

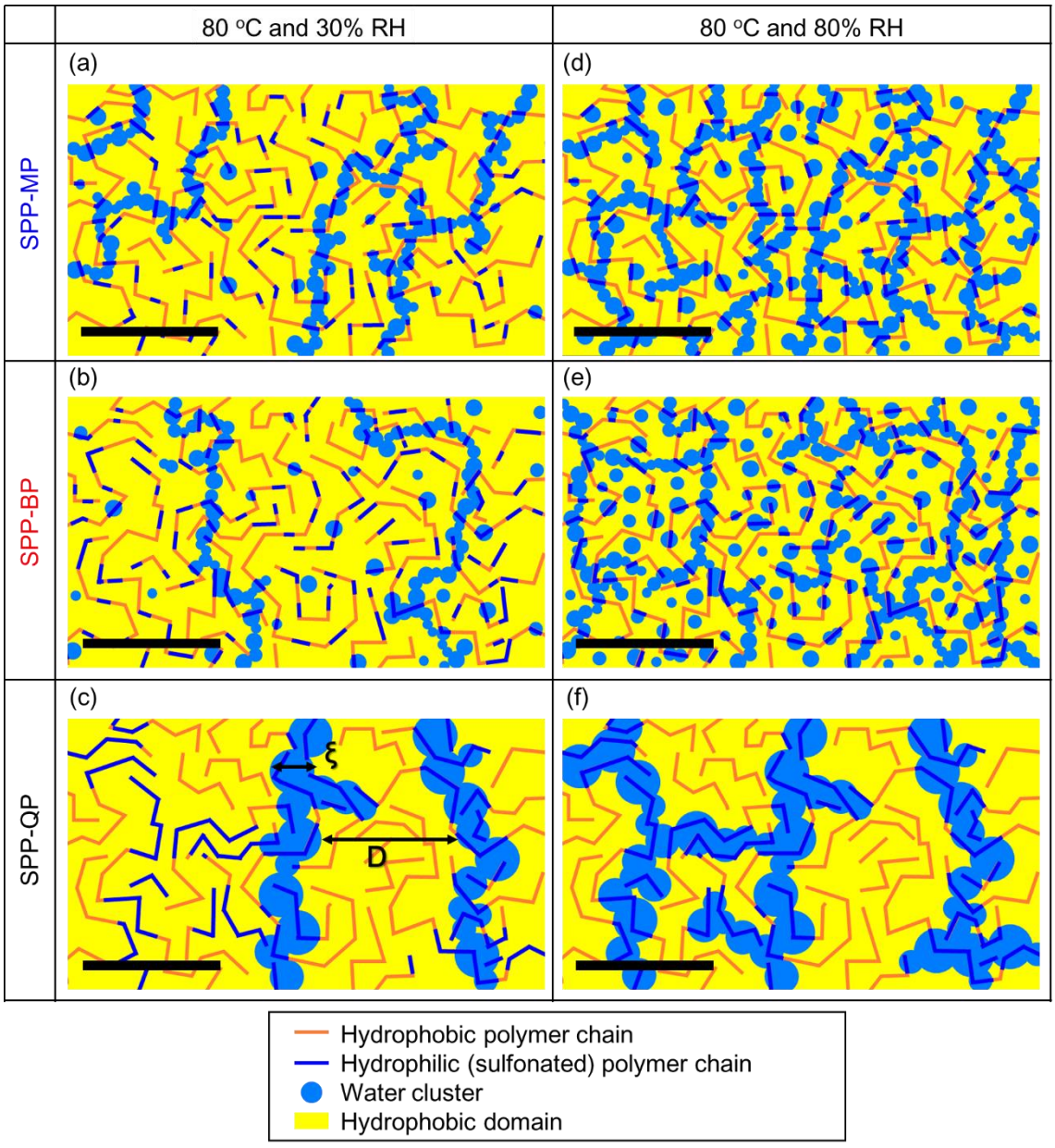

Figure 3-6 Morphological models of SPP-MP, SPP-BP, and SPP-QP membranes at 80 °C and (a-c) 30% RH and (d-f) 80% RH. For recognition, the black bar in each illustration is 4 nm long.

3.3.2 Water Uptake and Proton Conductivity

Liquid water uptake of the membranes was measured at 40 °C. The gravimetric and volumetric water uptake were 50 and 25% for SPP-MP, 39 and 27% for SPP-BP, and 79 and 20% for SPP-QP, respectively. Then, water uptake and proton conductivity of the membranes were measured at 80 °C and are plotted as a function of the humidity as shown in Figure 3-7. The three membranes showed similar humidity dependence of the water uptake from 20 to 95% RH. The SPP-MP membrane exhibited a higher water uptake (in particular, at high RH) than those for the SPP-BP and SPP-QP membranes because of the higher IEC of SPP-MP (2.5 mequiv. g^{-1}) than those of SPP-BP and SPP-QP (2.4 mequiv. g^{-1}). As shown in Figure 3-8, proton conductivity was replotted as a function of λ (number of absorbed water molecules per sulfonic acid group). SPP membranes with higher randomness of the SP unit exhibited lower proton conductivity at all λ values. To discuss the water absorbing properties in more detail, λ is plotted as a function of humidity (Figure 3-9). The λ values were in the order, SPP-MP > SPP-QP > SPP-BP. Since membranes with higher IEC tend to swell more, the SPP-MP membrane showed the largest λ value. Compared to SPP-BP, the SPP-QP membrane with the same IEC showed a larger λ value, presumably because of the higher interconnectivity of the water clusters (ξ/D). The proton conductivity was approximately in the order, SPP-QP > SPP-MP > SPP-BP, unlike that of water uptake. It is well-recognized that the proton conductivity of PEMs depends significantly on the morphology. We have recently reported that some polyphenylene-based PEMs with lower randomness of the hydrophilic components contained higher uniformity in the phase-separated morphology and thus exhibited higher proton conductivity [(11)]. In the present study, to understand the conductivity/morphology relationship more quantitatively, proton conductivity is replotted as a function of ξ/D

value as shown in Figure 3-10. At any humidity investigated, a linear relationship was obtained, indicating that the proton conductivity was dominated by the connectivity of the water clusters. The SPP-QP membrane with smaller randomness of the SP unit contained higher connectivity of the water clusters even at low humidity, resulting in higher proton conductivity compared to the other two membranes sharing the same chemical components and similar IEC values. Further investigation of the water dynamics using pulse-field gradient spin-echo NMR and/or inelastic neutron scattering will be taken up as a future work.

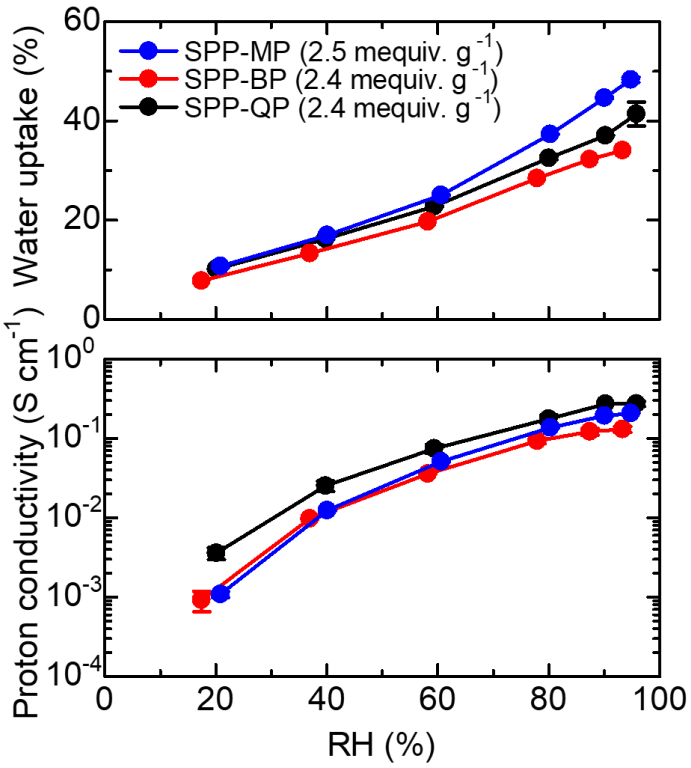

Figure 3-7 Water uptake and proton conductivity of SPP-MP, SPP-BP, and SPP-QP membranes at 80 °C.

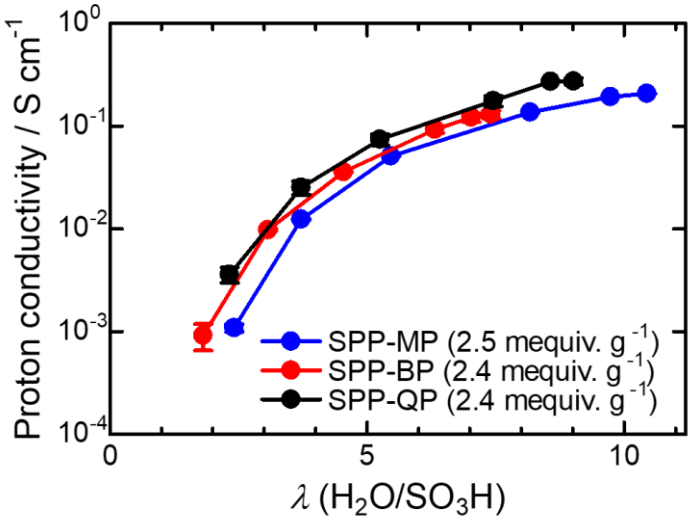

Figure 3-8 Proton conductivity of SPP-QP, SPP-BP, and SPP-MP as a function of number of absorbed water molecules per sulfonic acid group (λ). The data for the SPP-QP and SPP-BP were obtained from our previous papers (SPP-QP, *Sci. Adv.* 2017, *3*, eaao0476; SPP-BP, *Chem. Commun.* 2019, *55*, 7073).

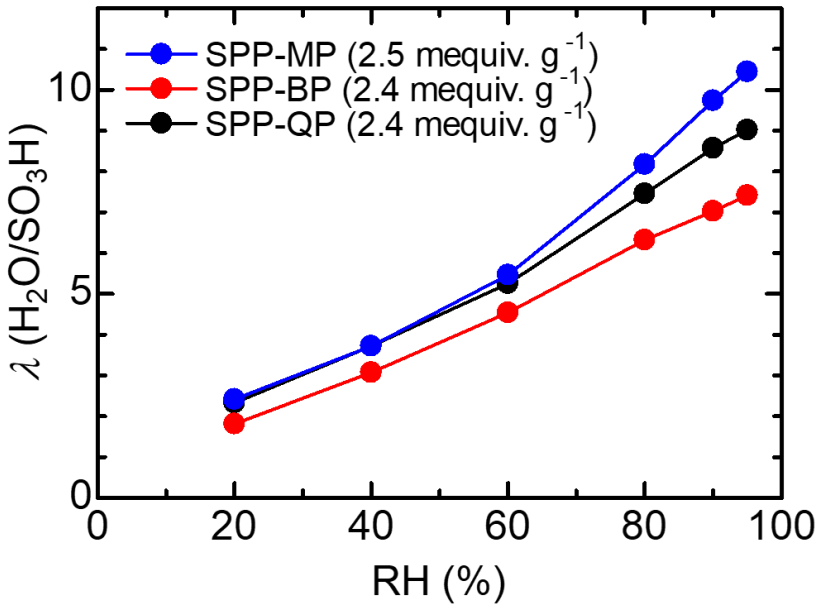

Figure 3-9 λ values of SPP-MP, SPP-BP, and SPP-QP membranes at 80 ºC as a function of the relative humidity (RH).

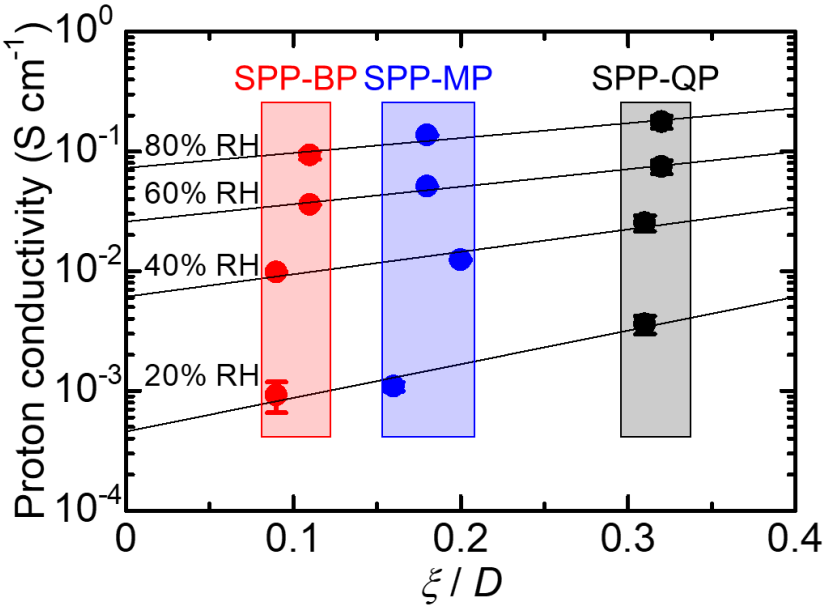

Figure 3-10 Proton conductivity of SPP-MP, SPP-BP, and SPP-QP membranes at 80 °C as a function of ξ/D (connectivity of the water clusters).

3.3.3 Mechanical Properties

Mechanical strength of the three membranes was evaluated by tensile testing at 80 °C, 20 and 60% RH, as shown in Figure 3-11 and Table 3-1. Under lower humidity (i.e., 20% RH), the Young's modulus and maximum stress of the SPP-MP membrane were 1.1 GPa and 54 MPa, respectively, which were comparatively high versus those of the SPP-BP (1.1 GPa and 31 MPa) or SPP-QP (1.1 GPa and 48 MPa) membranes. In contrast, the elongation properties differed among the three membranes, that is, the elongation at break was in the order SPP-BP (4%) < SPP-MP (9%) < SPP-QP (39%), suggesting that the elongation properties under low humidity were dominated by the connectivity of the water clusters due to insufficient hydration. At a more typical humidity (i.e., 60% RH), the elongation at break was improved and changed to the order SPP-MP (11%) < SPP-BP (40%) < SPP-QP (68%), in contrast to the similarity of Young's modulus and maximum stress of the three membranes being comparable to those of the 20% RH condition (1.1 GPa and 40 MPa for SPP-MP, 1.4 GPa and 43 MPa for SPP-BP, and 1.3 GPa and 41 MPa for SPP-QP). The effect of the molecular weight would be limited and was not accountable; the molecular weight was in the order SPP-QP (Mn = 7.3 kDa, Mw = 74.9 kDa, PDI = 10.3) < SPP-MP (Mn = 12.9 kDa, Mw = 98.8 kDa, PDI = 7.7) < SPP-BP (Mn = 25.6 kDa, Mw = 114.1 kDa, PDI = 4.5). The elongation at break was more related with the sequence of the polymer component and decreased linearly with the increasing randomness of the SP unit (Figure 3-12). Previously, we supposed that the lower randomness of the SP unit led to a well-sequenced hydrophobic structure, resulting in better mechanical properties [(11)]. This supposition has been supported in the present study via the abovementioned SANS-based morphological analyses and stress/strain properties. The SPP-QP membrane, with the lowest randomness of the SP unit, contained the largest

and best ordered hydrophobic domains, resulting in the highest elongation at break. It should be noted that the mechanical properties of our polyphenylene membranes were much superior to those (tensile stress of ~30 MPa, elongation at break of ~15%) of other polyphenylene-based membranes such as poly(phenylene benzophenone)s (all *para*-phenylene linkages in the main chain) [(1)], owing to the balanced combination of *meta*- and *para*-phenylene linkages.

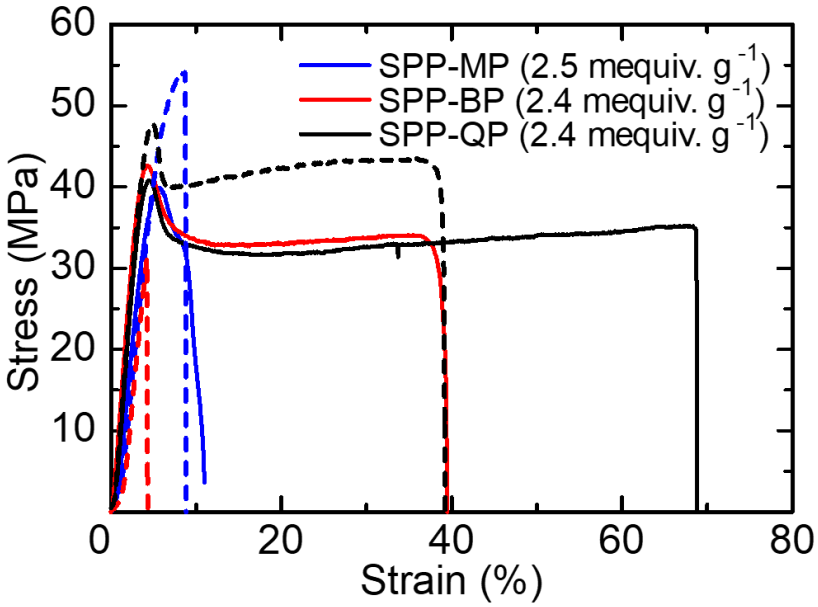

Figure 3-11 Stress versus strain curves of SPP-MP, SPP-BP, and SPP-QP membranes at 80 °C, 20% RH (dashed line) and 60% RH (solid lines).

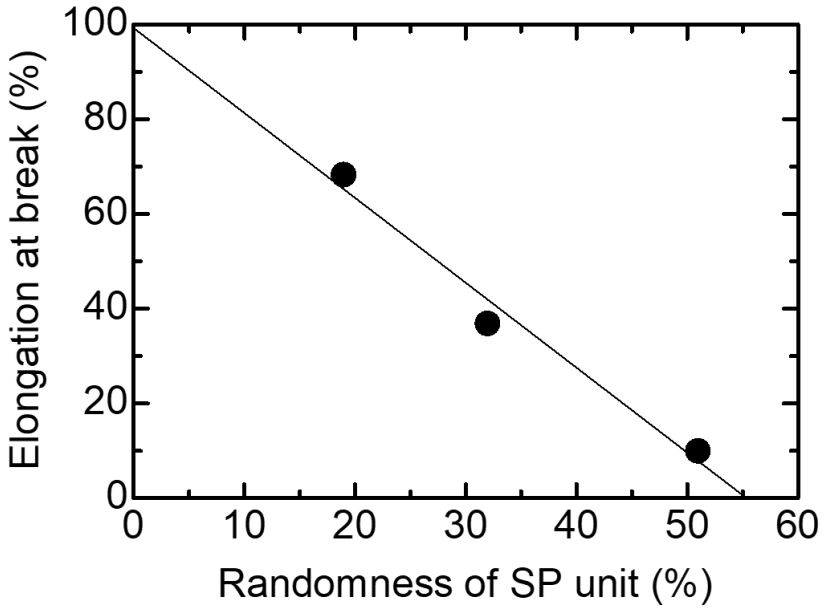

Figure 3-12 Elongation at break of SPP-MP, SPP-BP, and SPP-QP membranes as a function of the randomness of SP unit.

Table 3-1 Tensile properties of SPP-MP, SPP-BP, and SPP-QP membranes at 80 °C, 20% and 60% RH.

Polymer	Young's modulus (GPa)		Maximum stress (MPa)		Elongation at break (%)	
	20% RH	60% RH	20% RH	60% RH	20% RH	60% RH
SPP-MP	1.1	1.1	54	40	9	11
SPP-BP	1.1	1.4	31	43	4	40
SPP-QP	1.1	1.3	48	41	39	68

3.4 Conclusion

This chapter describes the relation between polymer structure and morphology/properties for three SPP ionomer membranes. The differences in the randomness affected the phase-separated morphology under dry conditions (as suggested by TEM images) only to a slight degree but affected the state (e.g., domain and interdomain size) of water clusters under humidified conditions to a large degree. Careful SAXS and SANS analyses under controlled humidity revealed that SPP-QP, with smaller randomness of the sulfophenylene units, contained more uniform, larger water clusters with higher interconnectivity. Increasing the humidity led to an increase in the number of water clusters but did not change their size, interdomain distance, or interconnectivity (ξ/D was 0.18 for SPP-MP, 0.11 for SPP-BP, and 0.31 for SPP-QP). The randomness of the SP units and the connectivity of the water clusters affected some membrane properties. The proton conductivity was correlated with the IEC values but more dominated by the interconnectivity of the water clusters over a wide range of humidity. The SPP-BP membrane, with lower connectivity, exhibited lower proton conductivity since isolated water clusters contained in this membrane did not contribute much to the proton conduction. Regarding the mechanical properties, while Young's modulus and maximum strain were comparable among the three membranes, the elongation at break improved linearly with the decreasing randomness of the SP units (11% for SPP-MP, 40% for SPP-BP, and 68% for SPP-QP). Through the present research, we have demonstrated an effective approach for improving some of the crucial properties of sulfonated polyphenylene membranes by controlling the sequence of the hydrophilic and hydrophobic components, without changing other parameters such as IEC, which had been believed to be more influential.

3.5 Reference

(1) Sutradhar, S. C.; Rahman, M. M.; Ahmed, F.; Ryu, T.; Lei, J.; Yoon, S.; Lee, S.; Jin, Y.; Kim, W. *J. Power Sources* **2019**, *442*, 227233.

(2) Skalski, T. J. G.; Adamski, M.; Britton, B.; Schibli, E. M.; Peckham, T. J.; Weissbach, T.; Moshisuki, T.; Lyonnard, S.; Frisken, B. J.; Holdcroft S. *ChemSusChem* **2018**, *11*, 4033-4043.

(3) Miyake, J.; Taki, R.; Mochizuki, T.; Shimizu, R.; Akiyama, R.; Uchida, M.; Miyatake, K. *Sci. Adv.* **2017**, *3*, eaao0476.

(4) Takata, S.; Suzuki, J.; Shinohara, T.; Oku, T.; Tominaga, T.; Ohishi, K.; Iwase, H.; Nakatani, T.; Inamura, Y.; Ito, T.; Suzuya, K.; Aizawa, K.; Arai, M.; Otomo, T.; Sugiyama, M. *JPS Conf. Proc.* **2015**, *8*, 036020-036025.

(5) Teubner, M.; Strey, R. *J. Chem. Phys.* **1987**, *87*, 3195-3200.

(6) Endo, H.; Mihailescu, M.; Monkenbusch, M.; Allgaier, J.; Gompper, G.; Richter, D.; Jakobs, B.; Sottmann, T.; Strey, R.; Grillo, I. *Chem. Phys.* **2001**, *115*, 580-600.

(7) Shiino, K.; Miyake, J.; Miyatake, K. *Chem. Commun.* **2019**, *55*, 7073-7076.

(8) Mochizuki, T.; Kakinuma, K.; Uchida, M.; Deki, S.; Watanabe, M.; Miyatake, K. *ChemSusChem* **2014**, *7*, 729-733.

(9) Narimani, R.; Yang, A. C. C.; Tsang, E. M. W.; Rubatat, L.; Holdcroft, S.; Frisken, B. J. *Macromolecules* **2013**, *46*, 9676-9687.

(10) Motokawa, R.; Annaka, M.; Nakahira, T.; Koizumi, S. *Colloids and Surfaces B: Biointerfaces* **2004**, *38*, 213-219.

(11) Hosaka, I.; Sawano, T.; Kimura, T.; Matsumoto, A.; Miyake, J.; Miyatake, K. *Bull. Chem. Soc. Jpn.* **2020**, *93*, 393-398.

Chapter 4 Synthesis and Properties of Sequenced Sulfonated Polyphenylene

4.1 Introduction

To obtain sulfonated polyphenylene membranes with improved properties, understanding the membrane morphology/property relationship is very important. As discussed in Chapter 3, the membrane properties such as proton conductivity and mechanical strength are altered by the randomness or sequence of sulfonated phenylene (SP) unit. Especially, the elongation at break of the sulfonated polyphenylene membranes was dependent on the sequence of the polymer component and decreased linearly with increasing the randomness of the SP unit.

Based on the results, the improvement of membrane properties might be expected by introducing the sequenced structures in the polymer backbone. In this chapter, two different synthetic processes for SPP-QP with more sequenced structure are proposed. Additionally, new sequenced hydrophilic monomer (BSP) was designed and applied to copolymerization with the QP monomer. The structure and membrane properties of the novel BSP-QP were investigated.

4.2 Experimental

4.2.1 Chemicals

3-Bromo-3'-chloro-1,1'-biphenyl, 5-amino-2-chlorobenzenesulfonic acid and 2,2-dimethyl-1-propanol were purchased from TCI, Inc. and used as received. 1,4-Phenylenediboronic acid, 2,5-dichlorobenzenesulfonic acid dihydrate [SP monomer], thionyl chloride [$SOCl_2$], bis(1,5-cyclooctadiene)nickel(0) [$Ni(cod)_2$], sodium nitrite [$NaNO_2$], pyridine, 2,2'-bipyridine, potassium carbonate [K_2CO_3], sodium carbonate [Na_2CO_3], bis(pinacolato)diboron, potassium iodide [KI], magnesium sulfate [Mg_2SO_4], lithium bromide [LiBr], dimethyl sulfoxide [DMSO], 1,2-dimethoxyethane [DME], *N*,*N*-dimethylformamide [DMF], thionyl chloride [$SOCl_2$], toluene, toluene dehydrate, methanol, ethanol, 2-propanol, tetrakis(triphenylphosphine)palladium(0) [$Pd(PPh_3)_4$], 0.01 M sodium hydroxide aqueous solution, hydrochloric acid, sodium chloride, acetic acid [EtOAc], chloroform [$CHCl_3$], chloroform-d_1 [$CDCl_3$], deuterated dimethyl sulfoxide [DMSO-d_6], activated carbon and celite were purchased from Kanto Chemical Co. and used as received. 1,1'-Bis(diphenylphosphino)ferrocene]dichloropalladium(II), complex with dichloromethane [$Pd(dppf)Cl_2 \cdot CH_2Cl_2$] was purchased from Sigma-Aldrich Co. LLC and used as received.

4.2.2 Measurement

^1H and ^{13}C NMR spectra, GPC profiles, titration IEC were measured according to chapter 2. TEM observation, SAXS measurement, water uptake and proton conductivity measurement, stress-strain curves test were conducted according to chapter 3.

4.2.3 Synthesis of QP monomer via a new synthetic route

A 300 ml one neck round-bottomed flask equipped with a condenser, a nitrogen purge and magnetic stirrer bar was charged with 3-bromo-3'-chloro-1,1'-biphenyl (18.7 mmol, 5.0 g), 1,4-phenylenediboronic acid (7.2 mmol, 1.2 g), K_2CO_3 (15.2 mmol, 2.1 g), degassed DME (40 ml), degassed DMF (20 ml) and degassed deionized water (20 ml). To the suspension, $Pd(PPh_3)_4$ (0.71 mmol, 0.82 g) was added. After stirring 90 ^oC for 24 hours, the reaction mixture was cooled to room temperature. The mixture was diluted with deionized water and off-white solid was obtained. The solid was washed with deionized water and methanol, dissolved in CH_2Cl_2 and purified by treating with activated carbon (ca. 1.0 g). After activated carbon and solvent were removed, the white solid was purified by reprecipitation from CH_2Cl_2/hexane. Finally, QP monomer was obtained as a crystalline white solid (3.54 mmol, 1.60 g, 49.1 % yield).

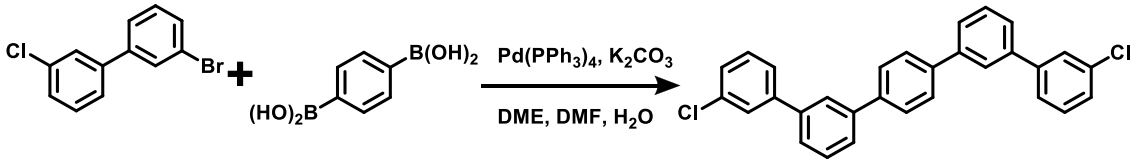

Scheme 4-1 Synthesis of QP monomer.

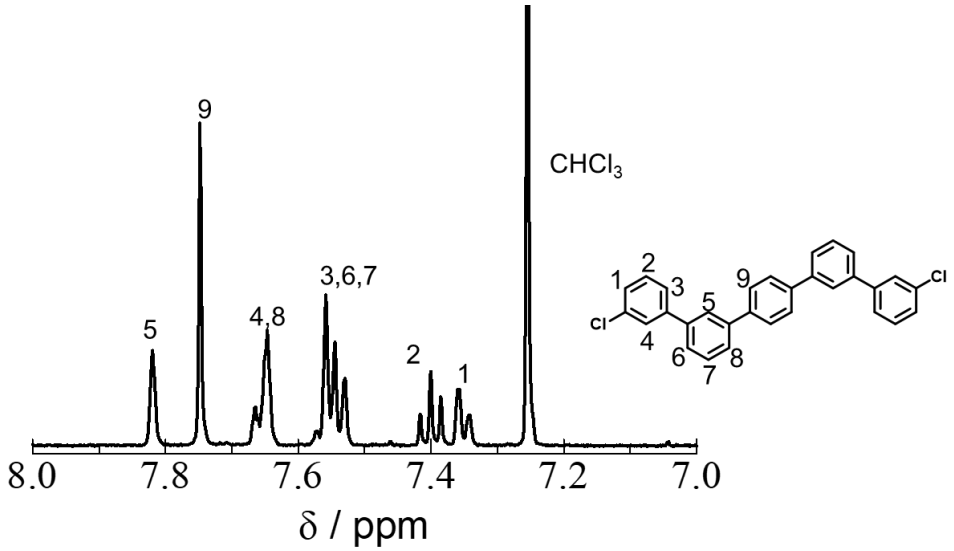

Figure 4-1 ^1H NMR spectrum of QP monomer via a new route in $CDCl_3$ at r.t.

4.2.4 Sandmeyer reaction of 5-amino-2-chlorobenzenesulfonic acid

5-Amino-2-chlorobenzenesulfonic acid (24.1 mmol, 5.00 g) were dissolved in water (40 ml), and Na_2CO_3 (12.1 mmol, 1.28 g) was added slowly until no further evolution of gas was observed. The solution was cooled to 0 °C, and $NaNO_2$ (26.6 mmol, 1.83 g) in water (7 ml) was added over period of 15 min. After stirring for 30 min, conc. HCl was added. Stirring was continued at 0 °C for 30 min, and then KI (20 mmol, 4.8 g) in water (20 ml) was added slowly. The solution was slowly heated to room temperature and then refluxed for 1 h. After cooling to room temperature, excess Na_2SO_3 was added to reduce residual iodine. Removal of the solvent and recrystallization from water gave pure sodium 2-chloro-5-iodobenzenesulfonate (16.7 mmol, 5.33 g, 69.4%).

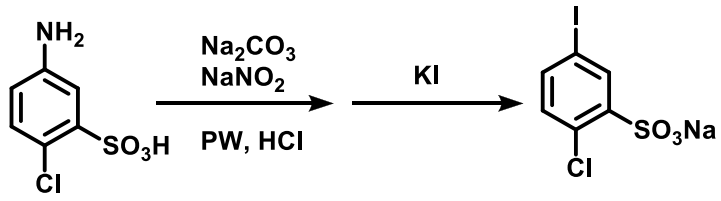

Scheme 4-2 Synthesis of sodium 2-chloro-5-iodobenzenesulfonate.

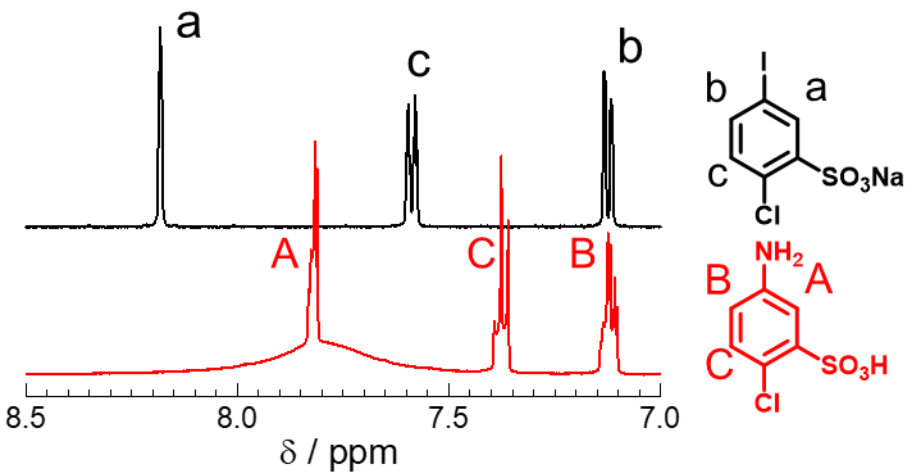

Figure 4-2 ^{1}H NMR spectra in DMSO-d_6 at 80 °C.

4.2.5 Synthesis of 2-chloro-5-iodobenzene-1-sulfonyl chloride

A pressure bottle equipped with a magnetic stirring bar was charged with sodium 2-chloro-5-iodobenzenesulfonate (18.8 mmol, 6.00 g) and $SOCl_2$ (12 ml). A DMF (0.5 ml) was poured slowly, and the solution was heated at 70 °C for 24 h. After the reaction, the mixture was cooled to room temperature, poured onto iced water and neutralized with sodium carbonate. The mixture was extracted with EtOAc and washed with brine. Then, the solvent was removed, and resulting product was dried in reduced pressure at 60 °C to give the target product in 85.0% yield (16.0 mmol, 5.39 g).

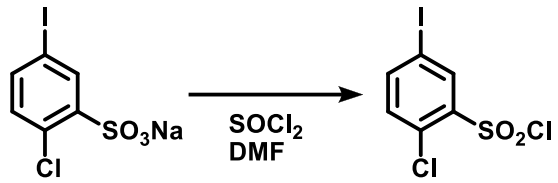

Scheme 4-3 Synthesis of 2-chloro-5-iodobenzene-1-sulfonyl chloride.

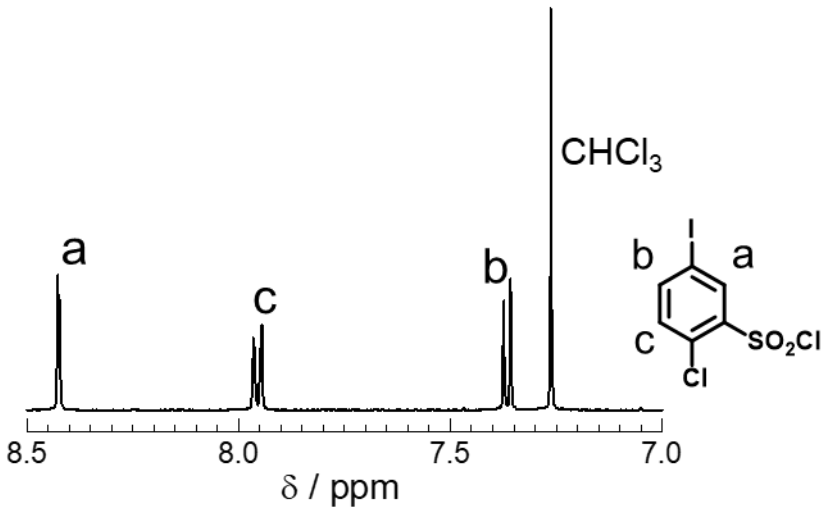

Figure 4-3 ^{1}H NMR spectrum of 2-chloro-5-iodobenzenesulfonyl chloride in $CDCl_3$ at r.t.

4.2.6 Protection reaction of 2-chloro-5-iodobenzenesulfonyl chloride

A 300 ml one-neck flask equipped with magnetic stirring bar was charged with 2-chloro-5-iodobenzenesulfonyl chloride (14.83 mmol, 5.00 g) and pyridine (100 ml). The mixture was cooled to 0 ^{o}C, and 2,2-dimethyl-1-propanol (44.49 mmol, 3.92 g) was added. The mixture was stirred at 0 ^{o}C for 1 h and room temperature for 18 h. After the reaction, the mixture was poured into 4 M HCl (400 mL) and extracted with EtOAc (300 mL). The organic layer was washed with saturated Na_2CO_3 aqueous solution and brine, and dried over Na_2SO_4 and filtrated through an activated carbon. The filtrate was concentrated using an evaporator. The residual solid was collected and dried in vacuum oven at 60 ^{o}C overnight gave the target product in 98.4% yield (14.6 mmol, 5.67 g).

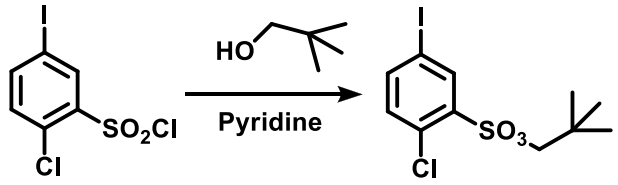

Scheme 4-4 Protection reaction of 2-chloro-5-iodobenzenesulfonyl chloride.

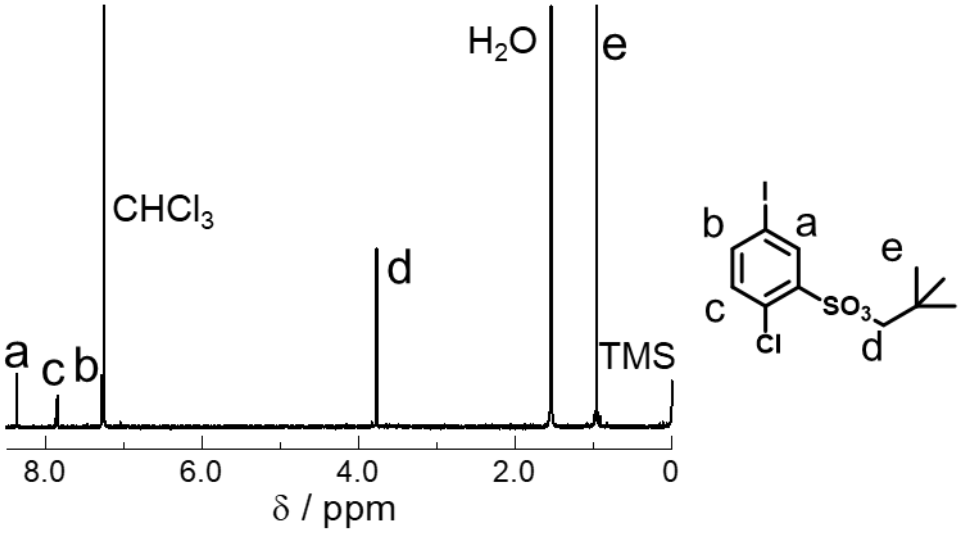

Scheme 4-4 ^{1}H NMR spectrum of neopentyl 2-chloro-5-iodobenzenesulfonate in $CDCl_3$ at r.t.

4.2.7 Synthesis of dineopentyl 4,4'-dichloro-[1,1'-biphenyl]-3,3'-disulfonate (BSP)

A 50 ml round-bottom flask equipped with a condenser was charged with neopentyl 2-chloro-5-iodobenzenesulfonate (11.8 mmol, 4.00 g), bis(pinacolato)diboron (5.91 mmol, 1.50 g), K_2CO_3 (17.7 mmol, 2.45 g), $Pd(dppf)Cl_2 \cdot CH_2Cl_2$ (0.06 mmol, 0.048 g), toluene (15 ml) and ethanol (6.0 ml). The mixture was heated to 70 °C and stirred for 24 h. The reaction mixture was diluted with water and $CHCl_3$, filtrated through a Celite plug, washed with water and concentrated. The resulting solid was purified by chromatography on silica gel (eluent: $CHCl_3$) and recrystallization (solvent: isopropanol) to give white solid in 59.4% yield (3.51 mmol, 1.84 g).

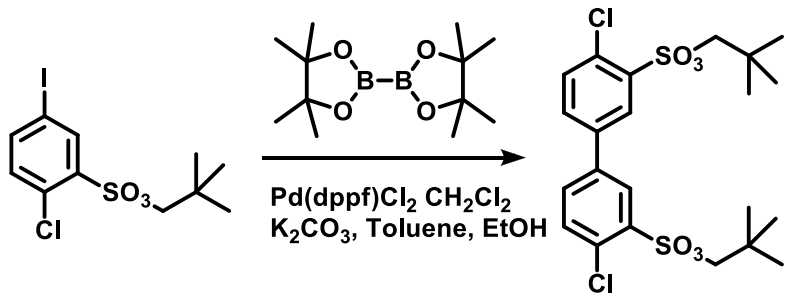

Scheme 4-5 Coupling reaction of neopentyl 2-chloro-5-iodobenzenesulfonate.

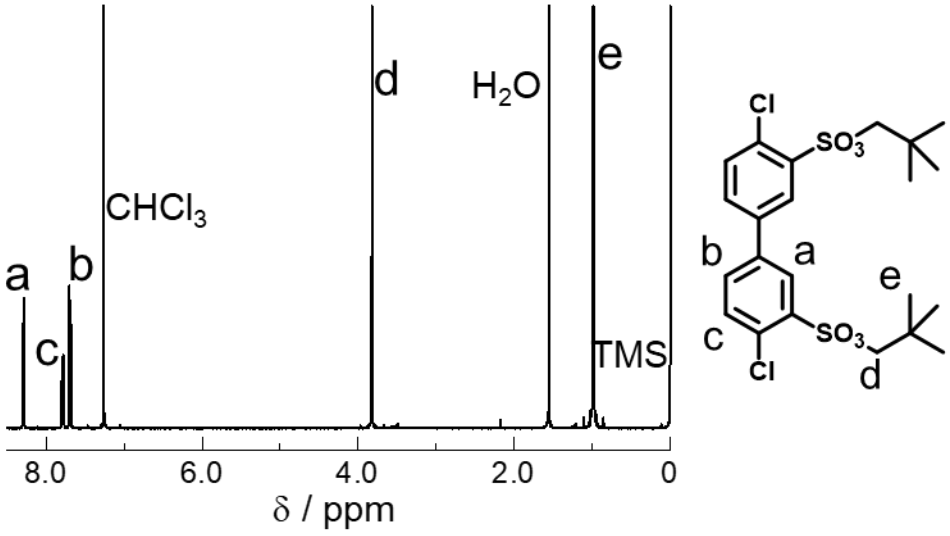

Figure 4-5 ^1H NMR spectrum of BSP monomer in $CDCl_3$ at r.t.

4.2.8 Synthesis of SPP-QP via two-step of the hydrophobic and hydrophobic monomers

A 100 ml three neck flask equipped with a reflux condenser, a Dean-Stark trap, a nitrogen inlet/outlet was charged with SP monomer (2.11 mmol, 0.552 g), 2,2'-bipyridine(9.55 mmol, 1.49 g), K_2CO_3 (2.32 mmol, 0.32 g), DMSO (18.4 ml) and toluene(10.0 ml). The mixture was heated at 170 °C for 2 hours for dehydration process. After removal of toluene, the reaction mixture was cooled to 40 °C followed by the addition of $Ni(cod)_2$ (9.09 mmol, 2.5 g), and then QP monomer(0.92 mmol, 0.415 g) was added 60 or 5 min later. After reaction for 3 hours at 80 °C, the reaction mixture was poured into methanol. The crude product was washed with 6 M hydrochloric acid (3 times) and water, and dried at 60 °C in vacuum overnight.

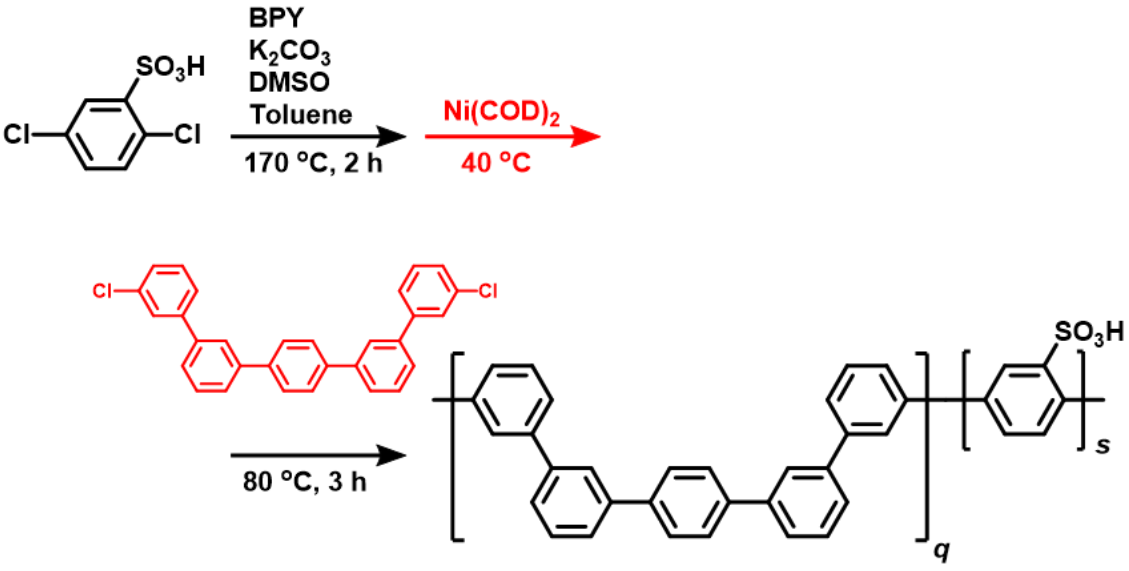

Scheme 4-6 Synthesis of SPP-QP via two-step addition of SP and QP monomers.

4.2.9 Synthesis of SPP-QP via two-step addition of the hydrophilic and hydrophobic monomer and $Ni(cod)_2$

A 100 ml three-neck flask equipped with a reflux condenser, a Dean-Stark trap, a nitrogen inlet/outlet was charged with SP monomer (0.951 mmol, 0.250 g), 2,2'-bipyridine (9.55 mmol, 1.49 g), K_2CO_3 (2.32 mmol, 0.32 g), DMSO (18.4 ml) and toluene (10.0 ml). The mixture was heated at 170 °C for 2 hours for dehydration process. After removal of toluene, the reaction mixture was cooled to 40 °C followed by the addition of $Ni(cod)_2$ (2.85 mmol, 0.785 g: 3.0 eq. to SP monomer). After stirring for 1 min, QP (0.92 mmol, 0.415 g) and $Ni(cod)_2$ (2.76 mmol, 0.753 g: 3.0 eq. to QP monomer) was added. After reaction for 3 hours at 80 °C, the reaction mixture was poured into methanol. The crude product was washed with 6 M hydrochloric acid (3 times) and pure water, and dried at 60 °C in vacuum overnight (in 81.4% yield).

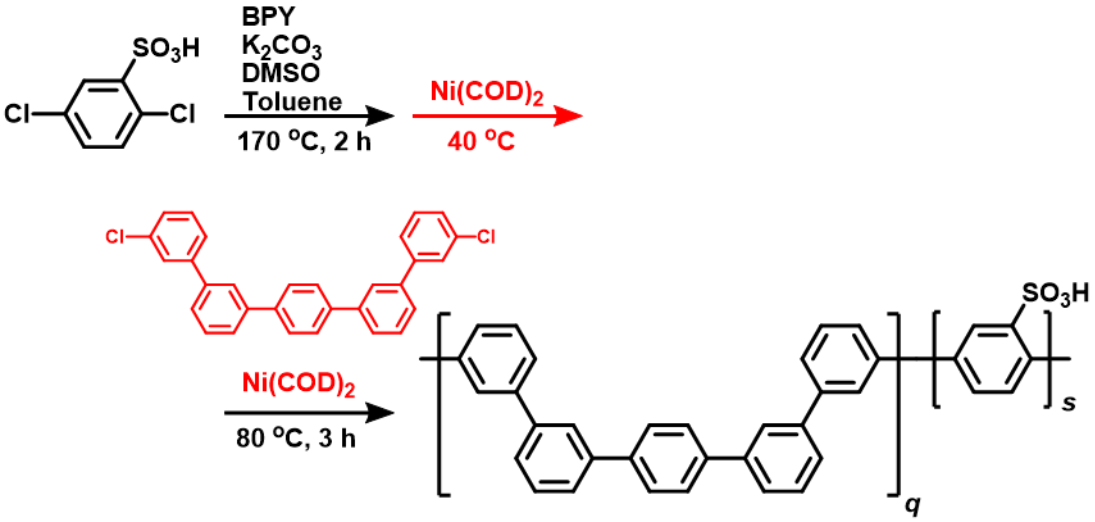

Scheme 4-7 Synthesis of SPP-QP via two-step addition of the hydrophilic and hydrophobic monomers and $Ni(cod)_2$.

.

4.2.10 Synthesis of BSP-QP via an in-situ deprotection reaction

A 100 ml three neck flask equipped with a reflux condenser, a Dean-Stark trap, a nitrogen inlet/outlet was charged with BSP monomer (0.501 mmol, 0.226 g) and LiBr (3.438 mmol, 0.298 g) and DMSO (5ml). The mixture was heated at 140 °C for deprotection reaction. After reaction for 3 h, QP monomer (0.42 mmol, 0.19 g), 2,2'-bipyridine (1.91 mmol, 0.30 g) and toluene (10 ml) were added, and the mixture was heated at 170 °C for 2 hours for azeotropic dehydration process. After removal of toluene, the reaction mixture was cooled to 80 °C followed by the addition of and $Ni(cod)_2$ (4.18 mmol, 1.15 g). After reaction for 3 hours, the reaction mixture was poured into methanol. The crude product was washed with 6 M hydrochloric acid (3 times) and deionized water (3 times). The polymer was recovered by filtration and dried at 60 °C in vacuum overnight (in 107% yield).

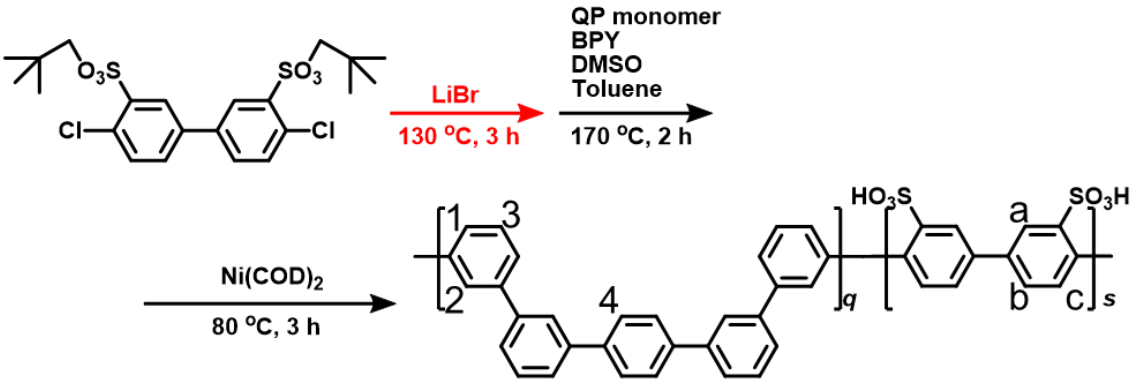

Scheme 4-8 Synthesis of the BSP-QP via an in-situ deprotection reaction.

4.3 Result and discussion

4.3.1 Synthesis of SPP-QP with later addition of hydrophobic monomer

To elucidate whether the different synthetic process using the same monomers (SP for hydrophilic and QP for hydrophobic component) for SPP-QP could change the randomness of SP unit, two different approaches were investigated. Firstly, delay method (Scheme 4-6) was conducted, i.e., QP was added after homo-polymerization of SP in certain period. More specifically, the QP was added 60 (run 1, Table 4-1) or 5 (run 2, Table 4-1) minutes after the addition of $Ni(cod)_2$. In the case of run 1, polymerization product was hardly soluble in organic solvents. The molecular weight was estimated to be small (M_n = 2.4 kDa, M_w = 4.5 kDa for run 1). The high yield (ca. 290%) is indicative of the remaining unreacted Cl-end groups. Shorter polymerization time for SP (5 minutes) increased the molecular weight and improved the solubility, but obtained polymer was not soluble completely in polar aprotic solvent such as DMSO, DMF and NMP (M_n = 4.9 kDa, M_w = 12.0 kDa for run 2). For further improvement of the solubility, the addition of promoter ($Ni(cod)_2$) was added in two step (Scheme 4-7), however, the resulting copolymer did not contain high enough molecular weight (M_n = 5.0 kDa, M_w = 8.3 kDa, run 3, Table 4-1). Overall, these two new synthetic approaches resulted in SPP-QP with significantly smaller molecular weight (thus membrane properties could not be evaluated), which stimulated me to try other approaches to decrease the randomness of SP unit for SPP ionomers.

Table 4-1 Copolymerization of the SPP-QP (run1-3) and BSP-QP (run 4).

Run	Polymer	IEC (mequiv. g^{-1})			Delay		Time for SP homo-polymerization	Molecular weight (kDa)[b]		Yield (%)	Solubility		Integral ratio of a_3[c]
		Feed	NMR	Titration	QP	$Ni(cod)_2$		M_n	M_w		DMSO	DMF	
-	SPP-QP[a]	2.8	2.6	2.6	1	1	-	39.4	145.0	97	○	○	0.00
1	SPP-QP	3.1	3.6[d]	3.4	2	1	60	2.4[d]	4.5[d]	290	×	×	-0.57
2	SPP-QP	3.1	2.7	2.5	2	1	5	4.9	12.0	91	△	△	-0.83
3	SPP-QP	3.1	1.5	1.5	2	2	1	5.0	8.3	81	○	○	-0.02
4	BSP-QP	3.1	3.0	2.9	1	1	-	30.4	149.5	107	△	△	-0.18

[a] Synthesized from QP monomer not include PCB. [b] Determined by GPC. [c] Calculated from ^{1}H NMR spectrum and titrated IEC value.
[d] Solubility part.

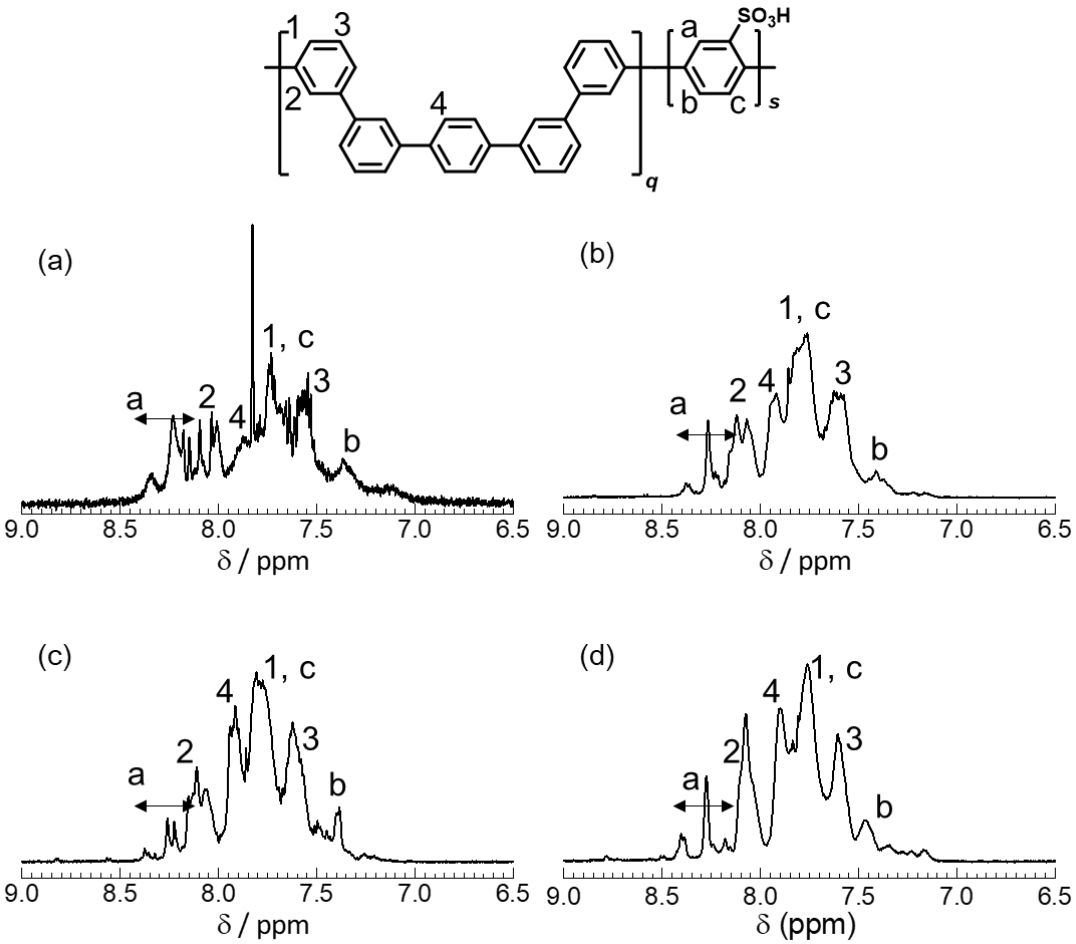

Figure 4-6 ^{1}H NMR spectra of the copolymers (a) run 1, (b) run 2 and (c) run 3 (d) SPP-QP in DMSO-d_6 at 80 °C.

4.3.2 Synthesis of BSP-QP

To lower the randomness of SP unit, a new copolymer (BSP-QP) was synthesized from new hydrophilic monomer (BSP monomer), which had biphenylene structure (Scheme 4-8). The BSP monomer was polymerized after an *in-situ* deprotection reaction with LiBr before the azeotropic dehydration process because the bulky protection groups presumably made the BSP monomer less reactive in the copolymerization reaction (run 4, Table 4-1). The progress of the in-situ deprotection reaction was monitored by TLC (eluent: acetic acid). The obtained BSP-QP copolymer was almost soluble in polar aprotic solvents (e.g., DMSO), had high molecular weights (M_n = 30.4 kDa, M_w = 149.5 kDa), and provided self-standing, brown and transparent membrane by solution casting (Figure 4-7(c)). In the ^{1}H NMR spectrum of the copolymer (run 4), the peaks assignable to the neopentyl protection groups completely disappeared, indicating that the successful deprotection reaction via the in-situ method. The IEC calculated from the ^{1}H NMR spectrum (2.9 mequiv. g^{-1}) was higher than that of SPP-QP (2.6 mequiv. g^{-1}).

The influence of the sequence length of hydrophilic monomer on polymer backbone was investigated. The hydrophilic component could take two configurations in this BSP-QP polymer, either connected with hydrophobic unit or hydrophilic unit (Figure 4-7 (d)). However, the assignment of these configurations were not available due to the complicated peaks and the randomness of SP unit was not estimated yet. The protons on the sulfonated phenylene groups need reassignment after more detailed analyses (e.g., assignment of low-molecular-weight model compounds and/or homopolymers).

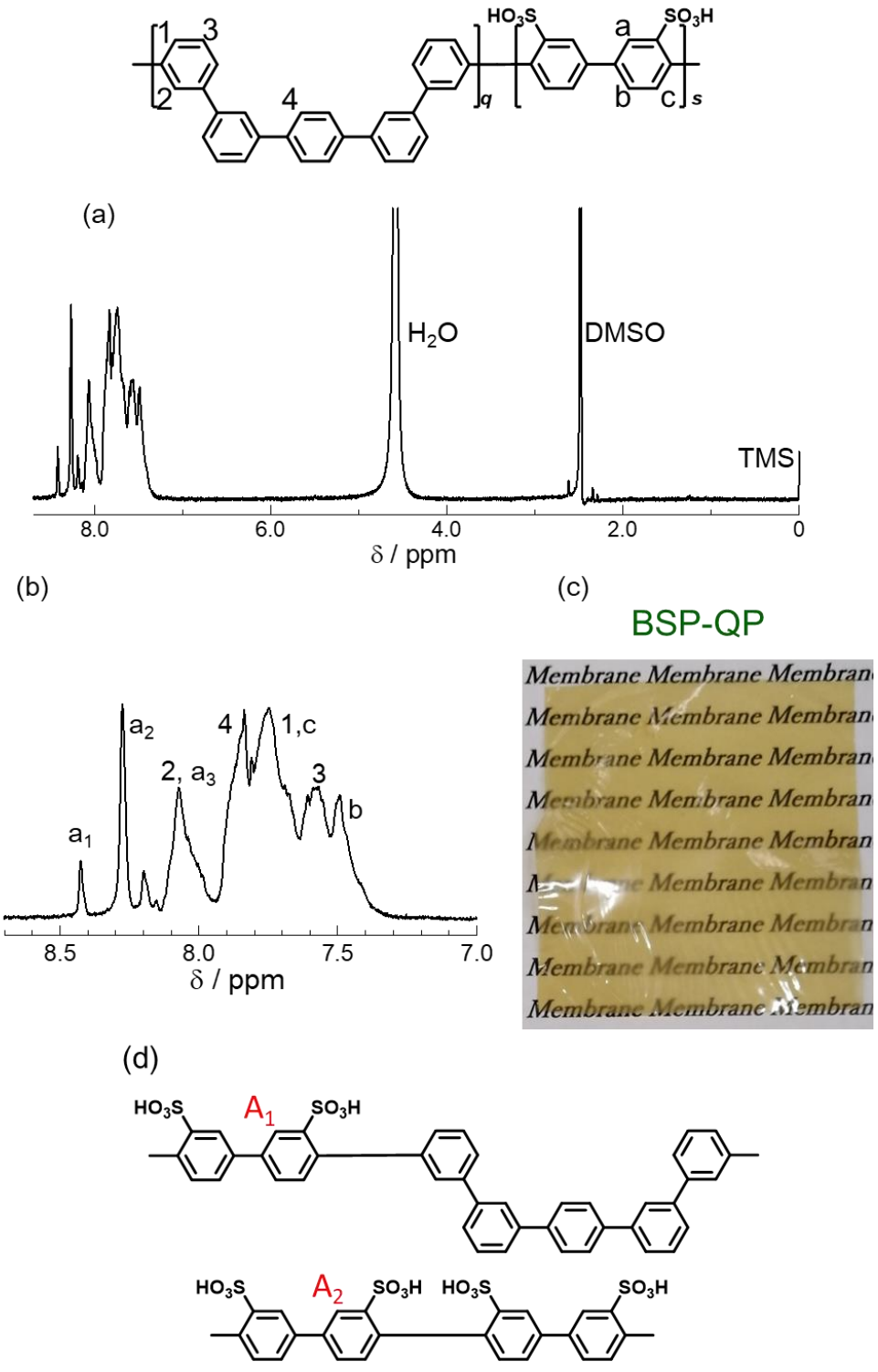

Figure 4-7 (a) ^{1}H NMR spectrum in DMSO-d_6 at 80 ^{o}C, (b) enlarged spectrum of (a), (c) photo image of BSP-QP synthesized via an in-situ deprotection reaction (run 4), and (d) possible sequences of the SP units.

4.3.3 Morphology

4.3.3.1 TEM observation

To discuss the influence of the sequenced structure in the hydrophilic part on the membrane morphology, TEM observation was carried out. Figure 4-8 shows the cross-sectional TEM images of BSP-QP (run 4) membrane stained with Pb^{2+} ions, in which the dark areas represent ionic clusters composed of the sulfonic acid groups and bright areas show hydrophobic domains. Under the dry conditions, the BSP-QP membrane showed hydrophilic-hydrophobic phase-separated morphology. The interface between the hydrophilic and hydrophobic domains were not distinct, similar to that of SPP-QP (2.4 mequiv. g^{-1}, see Figure 3-1). The size of hydrophilic and hydrophobic domains was slightly smaller (ca. 2.2 ± 0.4 nm for hydrophilic and 2.2 ± 0.4 nm for hydrophobic in diameter) than that (ca. 2.8 ± 0.2 nm for hydrophilic and 2.7 ± 0.8 nm for hydrophobic in diameter) of SPP-QP. The sequenced monomer also increase the length of hydrophobic sequence. The formation of larger clusters was probably inhibited by reduced electrostatic interactions due greater distances between the hydrophilic domains, resulting in small domain size under dry condition [(1)].

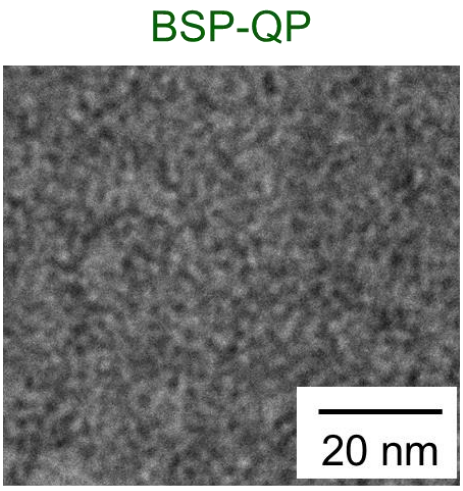

Figure 4-8 TEM image of BSP-QP (run 4, IEC = 2.9 mequiv. g^{-1}) membrane stained with Pb^{2+} ions.

4.3.3.2 SAXS measurement

SAXS measurement was carried out to estimate the morphology of BSP-QP membrane under controlled humidity conditions from 10% to 70% relative humidity (RH) at 80 ºC (Figure 4-9). As the humidity increased, the scattering intensity decreased similar to SPP-QP. The result suggest that absorbed water was located not only in the hydrophilic domains but also to some extent in the hydrophobic ones, resulting in the randomization of the phase-separated morphology [(2)]. BSP-QP showed a peak at ca. 10.3 nm of the d-spacing (or q = ca. 0.61 nm^{-1}) at 10 % RH, which was clearer and larger than that of SPP-QP (ca. 8.0 nm of the d-spacing or ca. q = 0.78 nm^{-1} at 30 % RH), suggesting that BSP-QP contained more-developed structure due to its sequenced hydrophilic (disulfo-biphenylene) monomer. From the background-subtracted profiles, the slopes in the Porod region was roughly estimated to be ca. -4 at 10% RH, suggesting that the structure was most likely to be spherical in BSP-QP membrane (Figure 4-10). These results suggested that the use of the sequenced monomer contributed to the development of more uniform and larger sized ionic clusters.

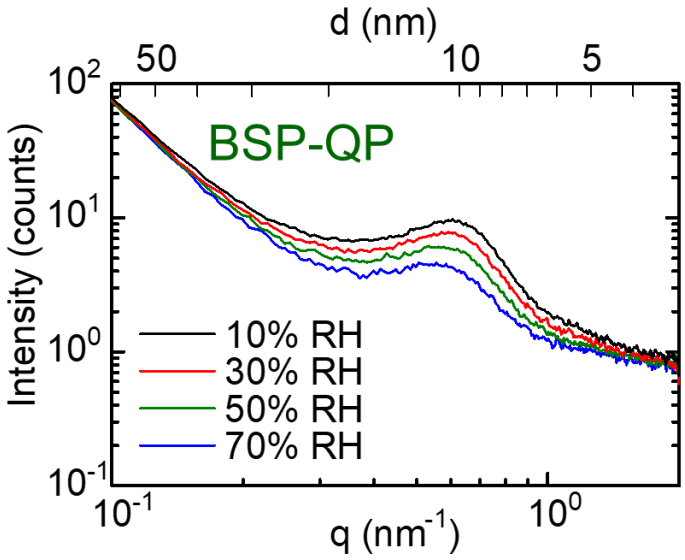

Figure 4-9 SAXS profiles for BSP-QP membrane as function of the q value at humidity from 10% to 70% RH and 80 ^{o}C.

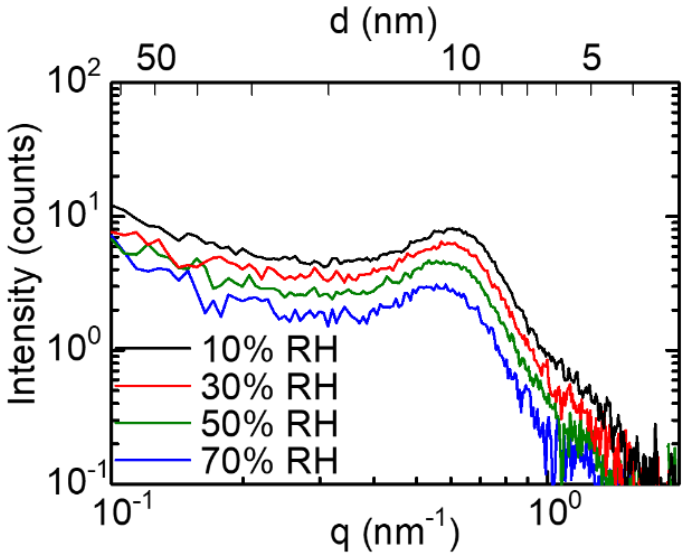

Figure 4-10 Background-subtracted SAXS profiles for BSP-QP as a function of the q value at relative humidity from 20 to 90% RH and 80 °C.

4.3.4 Water uptake and proton conductivity

Figure 4-11 shows the humidity dependence of water uptake and proton conductivity of the BSP-QP (IEC = 2.9 mequiv. g^{-1}, run 4) membrane at 80 ^{o}C. For comparison, data for SPP-QP membrane (IEC = 2.6 mequiv. g^{-1}) are also included. Be advised that the SPP-QP used herein was synthesized via the new synthetic route (as shown in Scheme 4-1). The water uptake and proton conductivity of the new SPP-QP were almost the same as those of our previous SPP-QP. BSP-QP membrane (run 4) showed higher water uptake than that of SPP-QP because of its higher IEC value. Consequently, the BSP-QP (run 4) exhibited much higher proton conductivity. The proton conductivity is replotted as a function of λ (number of absorbed water molecules per sulfonic acid group) in Figure 4-12. At any λ, the proton conductivity of BSP-QP was higher than that of SPP-QP, suggesting that the sequenced biphenylene hydrophilic monomer was suitable for proton conduction.

.

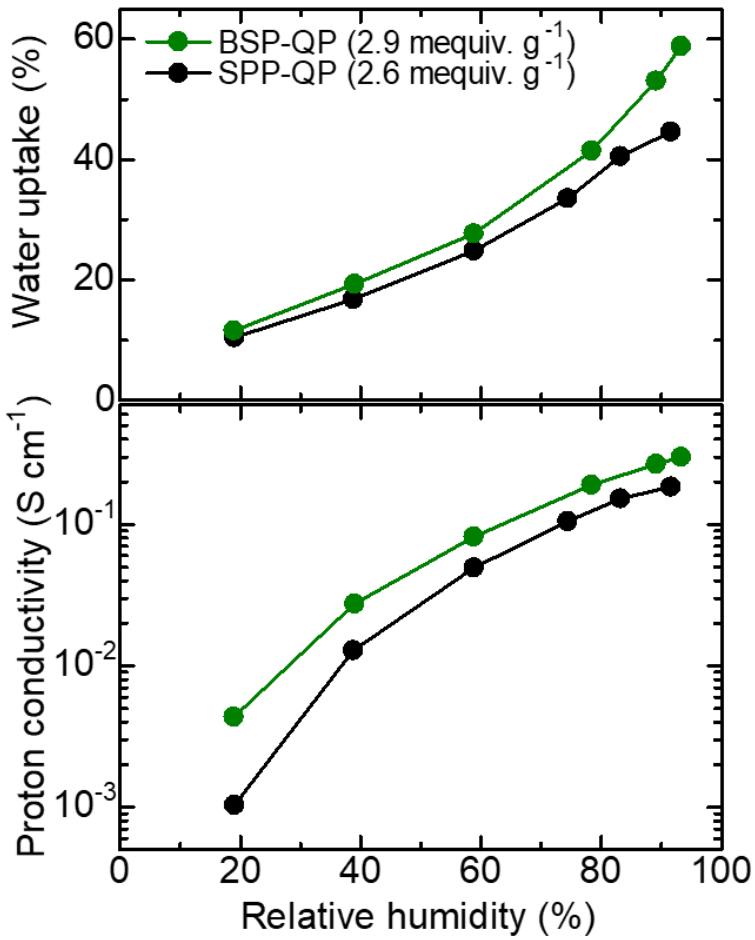

Figure 4-11 Water uptake and proton conductivity of BSP-QP (run 4) and new SPP-QP at 80 °C.

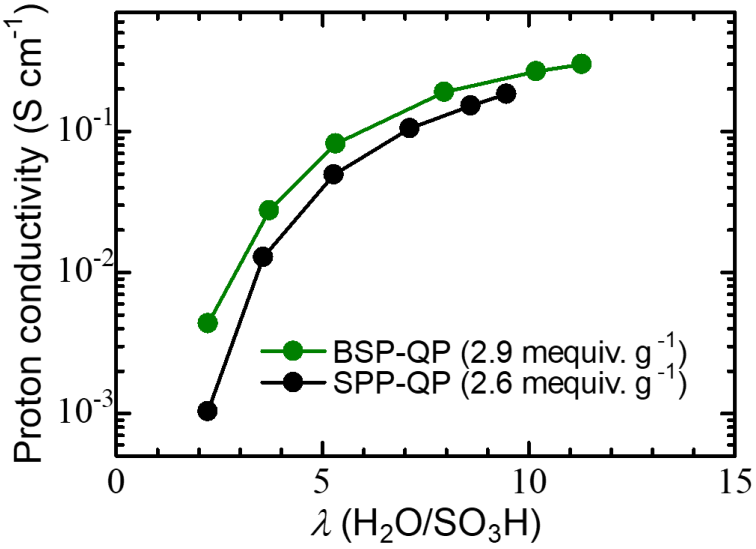

Figure 4-12 Proton conductivity of BSP-QP (run 4) and new SPP-QP at 80 °C as a function of λ.

4.3.5 Mechanical strength

Mechanical properties of BSP-QP membrane was measured by tensile test at 80 °C and 60% RH (Figure 4-13). Young's modulus and maximum stress of BSP-QP were 0.7 GPa and 25 MPa, respectively, which were comparable to those of SPP-QP (0.9 GPa of Young's modulus and 30 MPa of maximum stress, respectively, Table 4-2). In contrast, the elongation at break was slightly larger (9%). Taking into account the comparable molecular weight (M_n = 30.4 kDa and M_w = 149.5 kDa for BSP-QP and M_n = 39.4 kDa and M_w = 145.0 kDa for SPP-QP, respectively), this result is probably because of the larger sequenced hydrophobic parts for BSP-QP.

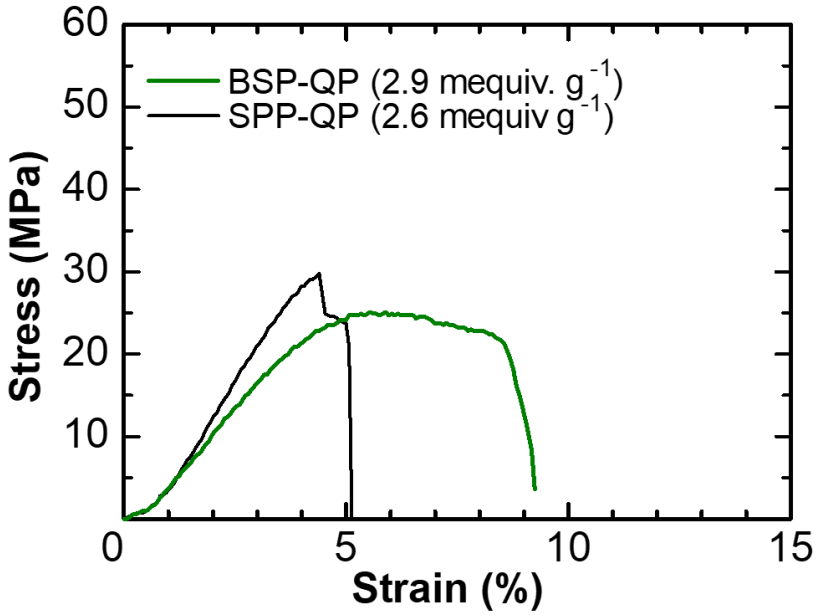

Figure 4-13 Mechanical strength of the BSP-QP (2.6 mequiv. g^{-1}) and SPP-QP (PCB free, 2.6 mequiv. g^{-1}) at 80 °C and 60% RH.

Table 4-2 Tensile properties of the BSP-QP (2.9 mequiv. g^{-1}) and SPP-QP (with high purity QP, 2.6 mequiv. g^{-1}) membranes at 80 °C and 60% RH.

Polymer	Young's modulus (GPa)	Maximum stress (MPa)	Elongation at break (%)
BSP-QP	0.7	25	9
SPP-QP	0.9	30	5

4.4 Conclusion

A process for synthesizing a sulfonated polyphenylene ionomer with large sequence length structure was investigated to achieve better-performing PEMs. In the two-step addition method, the resulting copolymer contained lower molecular weight. In contrast, a new copolymer (BSP-QP) from pre-sequenced, disulfobiphenylene hydrophilic monomer provided flexible membrane. BSP-QP showed well-developed phase-separated morphology as confirmed by SAXS measurement. The BSP-QP membrane showed somewhat better membrane properties such as proton conductivity and mechanical strength, compared with SPP-QP membrane. Although it is well-known that the too lager phase-separation morphology like block copolymer causes low catalyst activity or catalyst utilization because of low proton transport due to decreasing the interfacial contact between the membrane and catalyst layer, further supporting the idea that the sequence structure both in the hydrophilic and hydrophobic components was effective for improving the membrane properties [(3)].

4.5 Reference

(1) Tsang, E. M. W.; Zhang, Z.; Yang, A. C. C.; Shi, Z.; Peckham, T. J.; Narimani, R.; Frisken, B. J.; Holdcroft, S. *Macromolecules* **2009**, *42*, 9467-9480.

(2) Mochizuki, T.; Kakinuma, K.; Uchida, M.; Deki, S.; Watanabe, M.; Miyatake, K. *ChemSusChem* **2014**, *7*, 729-733.

(3) Mochizuki, T.; Uchida, M.; Uchida, H.; Watanabe, M.; Miyatake, K. *ACS Appl. Mater. Interfaces* **2014**, *6*, 13894-13899.

Chapter 5 General conclusions and Future prospects

5.1 General conclusions

It has been considered that sulfonated polyphenylene ionomers have a potential as an electrolyte membrane for PEMFCs, however, there have still been no membranes fulfilling required properties: high proton conductivity, gas impermeability, chemical stability and mechanical strength (in particular, elongation at break). This PhD research has demonstrated, for the first time, the guideline to improve those relevant properties of the polyphenylene ionomer membranes based on the monomer sequence in the polymer chains. The structure of water clusters (number, size, interdomain distance, interconnectivity, etc.) and hydrophobic domains dominate membrane properties, both of which can be adjustable by the monomer sequence in the polymer chains.

In Chapter 2, the effect of composition of hydrophobic monomer on molecular weight and membrane forming capability of the polymers (SPP-BP) using biphenylene (BP) as the hydrophobic component was investigated. Increasing *p* phenylene content in the SPP-BP caused larger molecular weights, however the solvent solubility decreased with increasing the *p*-phenylene content. The SPP-BPs with *m*/*p* phenylene ratio lower than 1 were not completely soluble in polar aprotic solvents due to strong interpolymer interactions caused by the high linearity of unsubstituted *p*-phenylene groups. Only the SPP-BP possessing *m*/*p* = 4/1 provided thin, bendable membrane, indicating that the balance of *m*/*p* phenylene composition (or persistence length, ca. l_p = 0.7 nm) is crucial for membrane forming capability. Then, the influence of the sequence length of the hydrophobic monomer (quinquephenylene (QP), BP and monophenylene (MP)) on

randomness of hydrophilic unit was investigated. The most remarkable difference among the three membranes (SPP-MP, -BP, -QP) is the randomness of sulfonated phenylene (SP) unit confirmed by ^{1}H NMR spectra and titrated IEC values. The randomness of SP unit was in the order of SPP-MP (51%) > SPP-BP (32%) > SPP-QP (19%), indicating that the hydrophobic monomer size dominates the sequence of the hydrophilic component.

In Chapter 3, the membrane morphology/properties of SPP-MP, SPP-BP and SPP-QP was carefully compared in terms of the randomness of SP unit discussed in Chapter 2. The effect of the randomness of SP unit on the phase-separated morphology under dry conditions (as suggested by TEM images) was negligible. In contrast, the structure of water clusters (number, size, interdomain distance, interconnectivity, etc.) confirmed by SAXS and SANS analyses under controlled humidity was dominated by the randomness of SP unit. The SPP-QP, with smaller randomness of the SP units, contained more uniform, larger water clusters with higher interconnectivity. Increasing the humidity resulted in an increase in the number of water clusters but did not change their size, interdomain distance, or interconnectivity. The randomness of the SP units or the connectivity of the water clusters affected some membrane properties. The proton conductivity was correlated mostly with the IEC values, and also influenced by the interconnectivity of the water clusters over a wide range of humidity. In contrast, the SPP-BP membrane, with lower interconnectivity of the water clusters, exhibited lower proton conductivity, because the isolated water clusters contained in the membrane did not contribute much to the proton conduction. Regarding the mechanical properties, while the Young's modulus and maximum strain were comparable for the three membranes, the elongation at break was improved linearly with decreasing randomness of the SP units.

In Chapter 4, a novel approach for synthesizing a sulfonated polyphenylene ionomer

with more sequenced structure was investigated to achieve better-performing polyphenylene ionomer membranes. Two-step addition of the monomers was conducted. Addition of the hydrophobic monomer afterwards provided only products with low molecular weight. In contrast, a new copolymer (BSP-QP) having disulfobiphenylene monomer as hydrophilic component provided flexible membrane. BSP-QP showed well-developed phase-separated morphology, confirmed by SAXS measurement. The BSP-QP membrane showed superior membrane properties such as proton conductivity and mechanical strength, compared with SPP-QP membrane, probably due to better inter-connected proton conductive pathway and larger sequenced hydrophobic components.

Through the present research, I have demonstrated an effective approach for improving some of the crucial properties of sulfonated polyphenylene membranes by controlling the sequence of the hydrophilic and hydrophobic components, without changing other parameters such as IEC, which had been believed to be more influential.

5.2 Future prospects

Based on my PhD research, the polyphenylene membrane properties such as proton conductivity or mechanical strength have been improved by changing the membrane morphology, especially the structure of the water clusters, which are controllable by introducing the sequenced comonomers without changes other factors such as the bulk concentration of the sulfonic acid groups (or IEC). For further improvement of PEMs, I propose three approaches.

1. Combination of a large sequenced hydrophilic monomer and introducing the higher *m*-phenylene composition for hydrophobic component.

More sequenced structure of polyphenylene main-chain may cause low solubility

because of the low local sulfonic acid group density and high linearity. Taking the membrane forming capability into account, polyphenylene ionomer needs to be dissolved in polar aprotic solvents such as DMSO or DMF and have high molecular weight. To solve these conflicting issues, I suggest that the combination of a large sequenced hydrophilic monomer and introducing the higher *m*-phenylene composition for hydrophobic component (Scheme 5-1). Large sequence length should lead large hydrophilic or hydrophobic domains by decreasing the randomness of SP unit, resulting in possibly improving proton conductivity and elongation at break. However, it is well known that the solubility of the polymer is greatly affected by the linearity of the main-chain and decreases with increasing the linearity of component [(1)]. Thus, the lower solubility due to decreasing the randomness of SP unit is compensated by increasing *m*-phenylene composition in the hydrophobic component. As described in Chapter 2, increasing *m*-phenylene composition caused low molecular weight because of small persistence length. By combining the large sequenced hydrophilic monomer and increased *m*-phenylene composition in hydrophobic monomer is expected excellent membrane properties.

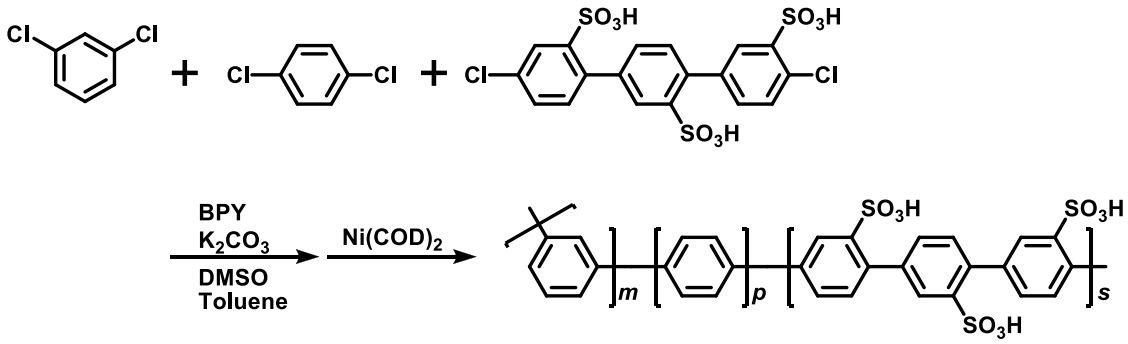

Scheme 5-1 Chemical structure of new terpolymer with large sequence hydrophilic monomer and higher *m*-phenylene composition ratio for hydrophobic component.

2. Effect of sequenced *p*-phenylene groups on membrane morphology.

In Chapter 3, the relationship of randomness of SP unit and membrane properties was shown. The influence of the connectivity of *p*-phenylene on membrane morphology should be also investigated to understand the polymer structure/properties relationship. The statistically estimated connectivity (sequence) of *p*-phenylene which was in the order SPP-QP > SPP-MP > SPP-BP probably affects the connectivity of proton conductivity pathway. By investigating of the *p*-phenylene connectivity/morphology relationship, we can obtain the insight to control the proton conductivity path morphology arbitrarily, and finally we have a strategy for high-performance sulfonated polyphenylene PEMs (Figure 5-1).

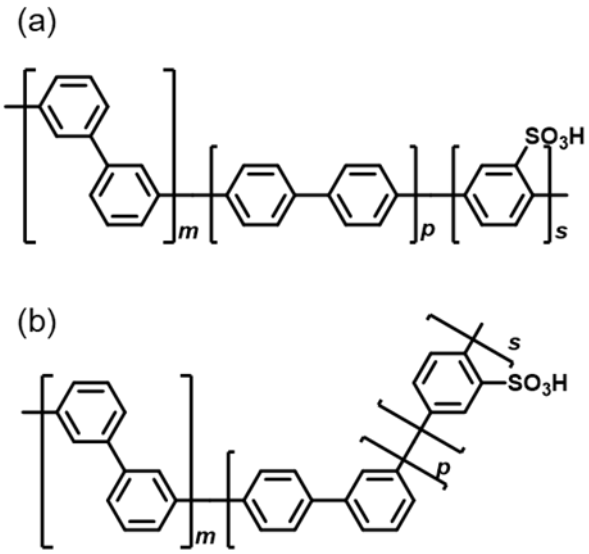

Figure 5-1 Chemical structure (a) SPP-BP and (b) new polymer with the same randomness of SP unit and different p-phenylene connectivity.

3. Introducing reinforcement material.

As described in chapter 3, the mechanical strength (or elongation at break) of the sulfonated polyphenylene membranes was mainly dominated by the randomness of the hydrophilic unit (see Figure 3-12). Thus, in terms of the molecular design, new sulfonated polyphenylene membranes with low randomness of the hydrophilic unit as possible sound promising. In addition, reinforcement with mechanical support layer would also be effective in improving the mechanical strength of the sulfonated polyphenylene membranes (Figure 5-2). By impregnating high IEC (or high connectivity of water cluster) polymer electrolyte into the reinforcement material, the composite membrane is expected to possess both high performance and mechanical strength, simultaneously [2, 3].

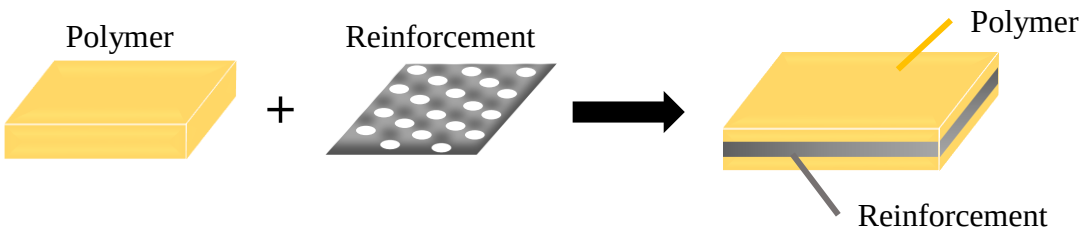

Figure 5-2 Image of reinforcement membrane.

5.3 Feasibility

The objective of this PhD research is to obtain the structural guideline for high performance proton exchange membranes (PEMs) for adopting the polymer electrolyte membrane fuel cells (PEMFCs). United States Department of Energy published the cost analysis of the 2017 projected fuel cell stack cost at 100000 systems / year, and electrolyte membrane dominated 12% of total production cost of PEMFCs (Figure 5-3) [(4)]. Development of PEMs with high performance and low cost can reduce the price and promote the wide spread dissemination of auto-mobile and stationary PEMFCs. Currently, the perfluorosulfonic acid (PFSA) based membranes have been used as PEMs, however, they have intrinsic disadvantages not only membrane properties but also high production cost because of the complicated synthesis process. The PEMs cost should be lower than 2000 JPY/m^2 to replace conventional internal combustion engine, however, the commercial price of the Nafion (ca. NRE212), the most successful commercialized PFSA, is 52200 JPY per 12 × 12 in^2 (561900 JPY/m^2) [(5, 6)]. Sulfonated polyphenylene developed in our laboratory, SPP-QP, is also expensive because this requires costly and air-sensitive $Ni(cod)_2$ or non-commercially available compound, quinque phenylene (QP) monomer. On the other hand, SPP-MP is potentially a low-cost membrane because this consist of only commercially available chemicals. The production cost of SPP-QP, SPP-BP and SPP-MP membrane was calculated using the following equation,

$$\text{Production cost (JPY/m}^2) = (\sum(C \times W)) \div Y \times \rho \times T \quad (5\text{-}1)$$

where *C* and *W* are the price and weight of the raw material, *Y* is the yield of the polymer, and ρ and *T* are the density and thickness of the polymer, respectively. The amount of $Ni(cod)_2$ and ρ were set to be 1.2 eq. to the reaction site (Cl) and 1.4 g/cm^3, respectively.

As the hydrophobic monomer size increased, the cost decreased, simply because the amount of the costly $Ni(cod)_2$ decreased with increasing the monomer size (i.e., the number of reaction site (molar amount of C-Cl bonding) was in the order SPP-MP > BP > QP). Inexpensive and easy-to-handle promoter alternative to $Ni(cod)_2$ is under investigation in our group. Our new promoter potentially decreases the polymer production cost drastically even in the laboratory scale.

The composite membrane in which PE is introduced as a reinforcement with 7 μm of thickness and 44% of porosity can provide the resulting membrane with high mechanical strength and lower the production cost by reducing the amount of polymer. The production cost of SPP-MP with PE reinforcement is 14,000 JPY/m^2. Moreover, in the case of Nafion, the price is reduced approximately 1/14 (40000 JPY/m^2) by purchasing on a large scale.[4] If the same cost reduction is achieved in SPP-MP, its price can be reduced to 1000 JPY/m^2 in simple calculation.

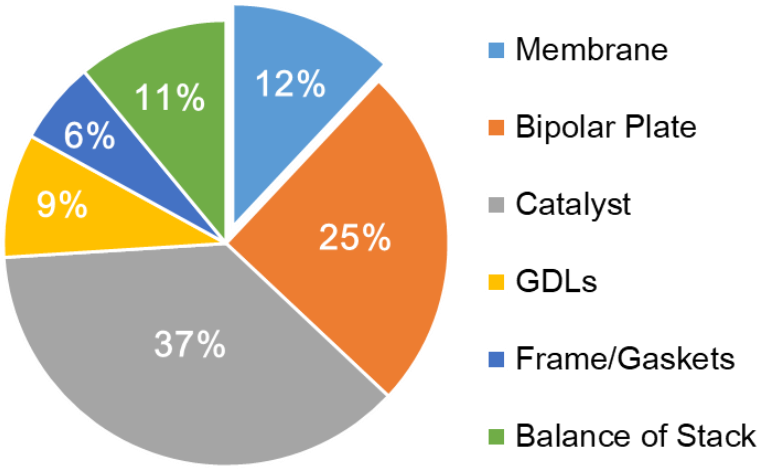

Figure 5-3 Cost analysis of the PEMFCs at 100000 systems per year.

Table 5-1 The cost of SPP series estimated based on the raw material.

	SPP-QP[a]	SPP-BP[a]	SPP-MP[a]	NRE212
$Ni(cod)_2$	950,000[c]	1,314,800[c]	1,873,500[c]	52,200[b] (561,900)[a]
New promoter	247,400[c]	155,100[c]	114,600[c]	
Composite membrane	30,500[d]	19,100[d]	14,000[d]	

[a] Unit is JPY/m^2. [b] Unit is JPY/in^2. [c] 50 μm thickness [d] 10 μm thickness.

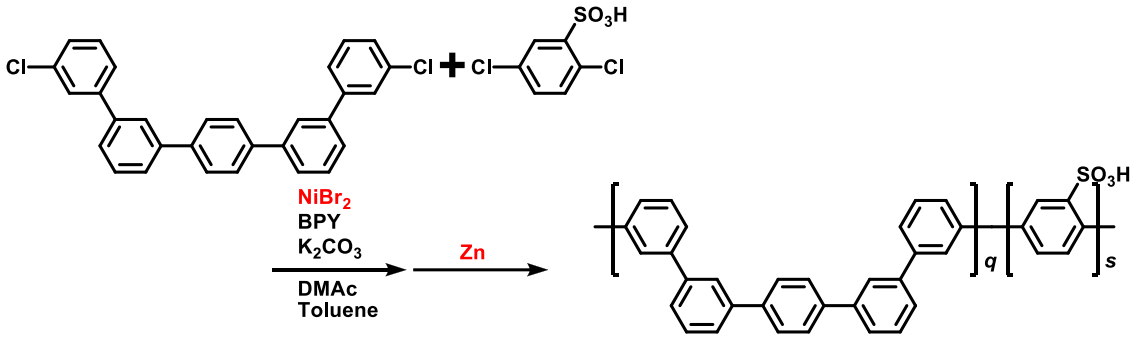

Scheme 5-2 Synthetic route of sulfonated polyphenylene ionomer using new promoter.

5.4 Reference

(1) Li, C.; Liu, M.; Pschirer, N. G.; Baumgarten, M.; Müllen, K. *Chem. Rev.* **2010**, *110*, 6817-6855.

(2) Miyake, J.; Kusakabe, M.; Tsutsumida, A.; Miyatake, K. *ACS Appl. Energy Mater.* **2018,** *1*, 1233-1238.

(3) Park, S.-G.; Chae, K.-J.; Lee, M. *J. Membr. Sci.* **2017**, *540*, 165-173.

(4) DOE Hydrogen and Fuel Cells Program Record “Fuel Cell System Cost -2017-”

(5) Merck HP

https://www.sigmaaldrich.com/catalog/product/aldrich/676470?lang=ja&region=JP

(6) NanotechJapan Bulletin Vol. 7, No. 4, 2014.

List of publications

1. Highly stable polyphenylene ionomer membrane from dichlorobiphenyls

   Keisuke Shiino, Junpei Miyake, Kenji Miyatake *Chem. Commun.* **2019**, *55*, 7073-7076.

2. Structural Investigation of Sulfonated Polyphenylene Ionomers for the Design of Better Performing Proton Conductive Membranes

   Keisuke Shiino, Toshiya Otomo, Takeshi Yamada, Hiroshi Arima, Kosuke Hiroi, Shinichi Takata, Junpei Miyake, Junji Inukai, Kenji Miyatake *ACS Appl. Polym. Mater.* **2020**, *2*, 5558–5565.

Meeting abstracts

1. 6th International seminar on green energy conversion, Nagano, Japan (2016.8)

   Keisuke Shiino, Toshihiro Miyao, Kazutoshi Higashiyama

2. 6th CSJ Chemistry Festa, Tokyo, Jalan (2016.11)

   Keisuke Shiino, Toshihiro Miyao, Higashiyama Kazutoshi

3. 13th European Congress on Catalysis, Florence, Italy (2017.8)

   Keisuke Shiino, Toshihiro Miyao, Hiroyuki Uchida, Akihiro Iiyama, Kazutoshi Higashiyama

4. 67th SPSJ Annual Meeting, Nagoya (2018.5)

   Keisuke Shiino, Junpei Miyake, Kenji Miyatake

5. The 7th International seminar on green energy conversion, Yamanashi, Japan (2018.8)

   Keisuke Shiino, Junpei Miyake, Kenji Miyatake

6. The 8th International Fuel Cell Workshop, Kofu, Japan (2018.8)

   Keisuke Shiino, Toshiya Otomo, Takeshi Yamada, Hiroshi Arima, Kosuke Hiroi, Shinichi Takata, Junpei Miyake, Junji Inukai, Kenji Miyatake

7. 68th Symposium on Macromolecules (2019.9)

   Keisuke Shiino, Toshiya Otomo, Takeshi Yamada, Hiroshi Arima, Kosuke Hiroi, Shinichi Takata, Junpei Miyake, Junji Inukai, Kenji Miyatake

8. 8th International seminar on green energy conversion, Kofu, Japan (2019.10)

   Keisuke Shiino, Toshiya Otomo, Takeshi Yamada, Hiroshi Arima, Kosuke Hiroi, Shinichi Takata, Junpei Miyake, Junji Inukai, Kenji Miyatake

Acknowledgments

This thesis is the summer of research at the clean Energy Research Center, Fuel Cell Nanomaterials Center and the Integrated Graduate School of Medicine, Engineering, and Agricultual Sciences at the University of Yamanashi, during 2017-2022. This research was supported by funds for the “Superlative, Stable, and Scalable Performance Fuel Cell” (Sper-FC) project from the New Energy and Industrial Technology Development Organization (NEDO).

I would like to express my deepest gratitude to **Professor Kenji Miyatake** of University of Yamanashi for this academic supervisor of this work, for his continuous guidance, invaluable suggestion, and warm encouragement thought the study.

I would like to express my gratitude to **Associate Professor Junpei Miyake** of University of Yamanashi for continuous supports, beneficial instructions and invaluable help and advices.

I would like to express my gratitude to **Professor Hiroyuki Uchida** and **Professor Akihiro Iiyama** of University of Yamanashi for warm encouragements, continuous consideration and kindness.

I would like to thank **Professor Hiroshi Irie,** and **Associate Professor Hideyuki Shinmori** of University of Yamanashi, and **Professor Hiroyoshi Kawakami** of Tokyo Metropolitan University for the helps as members of the advisory committee.

Sincere gratitude is expected to **Professor Kazutoshi Higashiyama** and **Professor Toshihiro Miyao** of University of Yamanashi for their support and encouragement.

My deep appreciation is expressed to **Dr. Toshiya Otomo** of Institute of Material Structure Science, High Energy Accelerator Research Organization, **Dr. Takeshi Yamada and Dr. Hiroshi Arima** of Neutron Science and Technology Center, Comprehensive Research Organization for Science and Society, and **Dr. Kousuke Hiroi** and **Dr. Shinichi Takata** of Materials & Life Science Facility Division, JPARC Center for experimental support and constructive advice.

I would like to express my thanks to **Professor Donald Alexander Tryk** and **Professor Manuel Eduardo Brito** for your kindness, helpful English support and useful advices.

I would like to express my gratitude **Professor Makoto Uchida, Professor Masahiro Watanabe, Professor Katsuyoshi Kakinuma, Associate Professor Shinji Nohara, Assistant Professor Hanako Nishino,** and **Assistant Professor Teppei Kawamoto** of University of Yamanashi for their support and encouragement.

I am grateful to **Professor Deborah Jones and Professor Jacques Rozière, Ms. Sara Cavaliere,** and **Mr. Spanu Francesco** of University of Montpellier for their kindly support and invaluable discussion.

I am grateful to **Dr. Akinobu Matsumoto, Dr. Ryo Akiyama, Ms. Toshiko Gomyo,** and **Ms. Mika Kodama** for technical supports and practical discussions.

I would like to thank **Dr. Yuji Chino, Dr. Yuya Yamashita, Mr. Takumi Kuroda, Mr. Jun Fukasawa, Dr. Hideaki Ohno, Mr. Ikkei Arima, Mr. Takashi Masuda, Dr. Ibuki Hosaka, Dr. Taro Kimura, Dr. Zhi Long, Mr. Kohei Uyama, Ms. Reika Oida, Mr. Yuta Oishi, Mr. Ueno Koki, Ms. Mizuki Hayashi, Dr. Hiromichi Nishiyama, Mr. Toshiki Tanaka, Mr. Takayuki Watanabe, Mr. Takatoshi Sawano, Mr. Yuto Shirase,** and **Mr. Ren Kumao** for their kindly support.

I would like to thank **Dr. Morio Chiwata, Dr. Takashi Mochizuki, Dr. Hideaki Ono, Dr. Kento Takahashi, Dr. Ryosuke Nishikawa, Dr. Ryo Shimizu, Ms. Chisato Arata, Mr. Shigefumi Shimada, Dr. Shun Kobayashi, Dr. Zhang Yaojian, Dr. Jinju Ahn, Mr. Ryo Shirasaka, Ms. Liu fanghua, Ms. Chinatsu Takayama, Mr. Guo Lin, Ms. Rutsu Tamura, Ms. Aki Kobayashi, Mr. Takashi Sato, Mr. Takumi Nagasaka, Mr. Yoshihiro Ozawa, Mr. Yuto Shikano, Mr. Makoto Yonenaga,** and **Mr. Ryohei Tomiyama** for their grateful support.

I would like to offer my special thanks to **Mr. Yu Kakizawa** and **Ms. Mizuki Ozawa**. Without their encouragements, my doctoral program would not have been possible.

Sincere gratitude is also expressed to **Ms. Nozomi Toyoda, Ms. Tomomi Hashizume,** and **Ms. Kaori Ichinose** and all staffs of Clean Energy Research Center, Fuel Cell Research Nanomaterials Center for their kind support and help.

I greatly appreciate the support of my family, **Tatsuo Shiino, Kunie Shiino, and Hirofumi Shiino** to their support and sincere encouragement.

Finally, I would like to express my heartily gratitude to **Ms. Marina Abe**, her support and sincere.

March 2021

Keisuke Shiino